RSC Advances

PAPER

View Article Online
View Journal | View Issue

Cite this: *RSC Adv.*, 2023, **13**, 24291

Molecular dynamics simulation approach of hybrid chalcone–thiazole complex derivatives for DNA gyrase B inhibition: lead generation†

Afroz Patan, [a] Vijey Aanandhi M.[a] and Gopinath P. *[b]

Received 3rd February 2023
Accepted 31st July 2023

DOI: 10.1039/d3ra00732d

rsc.li/rsc-advances

Compounds bearing thiazole and chalcone groups have been reported to be excellent leads for antibacterial, antitubercular and anticancer activities. In view of this, we performed quantitative structure–activity relationship studies using QSARINS for dataset preparation and for developing validated QSAR models that can predict novel series of thiazole–chalcone hybrids and further evaluate them for bioactivities. The molecular descriptors AATS8i, AVP-1, MoRSEE17 and GATSe7 were found to be active in predicting the structure–activity relationship. Molecular docking and dynamics simulation studies of the developed leads have shown insights into structural analysis. Furthermore, computational studies using AutoDock and Desmond predicted the key binding interactions responsible for the activity and the SwissADME tool computed the *in silico* drug likeliness properties. The lead compound 178 generated through this study creates a route for the optimization and development of novel drugs against tuberculosis infections. RMSD, RMSF, RoG, H-bond and SASA analysis confirmed the stable binding of compound 178 with the 6J90 structure. In addition, MM-PBSA and MM-GBSA also confirm the docking results. We propose the designed compound 178 as the best theoretical lead, which may further be experimentally studied for selective inhibition.

Introduction

Although most pharmaceuticals have heterocyclic rings, their chemistry is crucial in the development of therapeutic compounds.[1] This illustrates how heterocyclic chemistry has influenced the design and development of potential therapeutics. Due to their many biological actions, organic and medicinal chemists have researched thiazole derivatives in great detail.[2,3] Many anti-cancer medications have a thiazole ring, including bleomycin, dasatinib, tiazofuran, and epothiolone B. Other thiazole-based drugs include sulfathiazole, ravuconazole, abafungin, acinitrazole, micrococcin, penicillins, cephalosporins, nitazoxanide, ritonavir, meloxicam, febuxostat, famotidine, nizatidine, pramipexole, chlormethiazole and thiamine. A class of open chain natural flavonoids called chalcones has potential biological properties. Chalcones are diaryl vinyl ketones serving as a crucial synthon for augmenting the pharmacological value, in addition to being responsible for the biological action of chalcones.[4,5]

A wide range of bioactivities, including anticancer,[5–19] antitubercular,[20–31] antifungal,[32–39] antioxidant[40–45] and antibacterial,[46–54] are present in thiazole and chalcone derivatives. The degree of a particular biological activity is determined by the type of aryl ring attached to the chalcone and the variety of substituents on the thiazole ring. Fluoro and chloro-substituted chalcones exhibit increased biological activity. Interestingly, the kinetic properties of drug-like candidates are improved by the insertion of halogen-modified aryl rings and heterocyclic structures.[55] Molecular hybridization for joining biologically active pharmacophoric groups is a strategy that will result in compounds with greater bioactivity.[56] In the past, thiazole–chalcone hybrids with therapeutic properties have been described.[57,58] In light of the aforementioned information, we generated and validated novel thiazole–chalcone hybrids incorporating biologically energetic thiazole and chalcone pharmacophores in an effort to identify new lead compounds with enhanced anticipated biological activities.

Experiment and methods

Multiple linear regression models were developed and generally validated by options available within the software QSARINS according to the chemometric approach.[59–61] The dataset series of forty-seven chalcone derivatives showing *Staphylococcus aureus* inhibition value were taken from the literature reported by Liaras *et al.*[62] and Geronikaki *et al.*[63] The dataset compounds were subjected to drug likeliness property checking by Lipinski's rule using the DRULITO tool. The IC_{50} values of the

[a]*Department of Pharmaceutical Chemistry, School of Pharmaceutical Sciences, VISTAS, Chennai, Tamil Nadu, India*

[b]*Department of Pharmaceutical Chemistry, GITAM School of Pharmacy, GITAM University, Hyderabad, Telangana, India. E-mail: gopi.pharma@gmail.com*

† Electronic supplementary information (ESI) available. See DOI: https://doi.org/10.1039/d3ra00732d

Table 1 Antibacterial activity of the dataset compounds against *Staphylococcus aureus*: structure, and experimental IC_{50} and pIC_{50} values

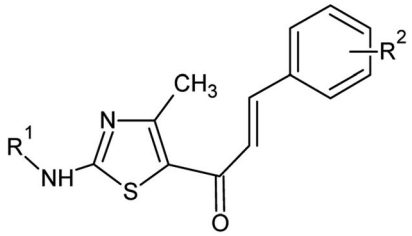

Compounds 1 to 27

Sl. no	R^1	R^2	Sl. no	R^1	R^2
1	CH_3	H	15	CH_3	2,3-diCl
2	CH_3	4-NO_2	16	C_2H_5	H
3	CH_3	3-NO_2	17	C_2H_5	4-NO_2
4	CH_3	4-Cl	18	C_2H_5	3-NO_2
5	CH_3	3-Cl	19	C_2H_5	4-Cl
6	CH_3	2-Cl	20	C_2H_5	3-Cl
7	CH_3	4-OCH_3	21	C_2H_5	2-Cl
8	CH_3	2-OCH_3	22	C_2H_5	4-F
9	CH_3	2,6-diCl	23	C_2H_5	3-F
10	CH_3	2,4-diCl	24	C_2H_5	3-Br
11	CH_3	4-F	25	C_2H_5	4-OCH_3
12	CH_3	3-F	26	C_2H_5	2-OCH_3
13	CH_3	3-Br	27	C_3H_7	H
14	CH_3	4-CH_3			

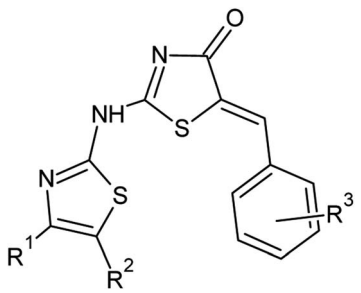

Compounds 28 to 47

Sl. no	R^1	R^2	R^3
28	H	H	3-OH
29	H	H	3,5-Dimethoxy, 4-OH
30	H	H	2-Methoxy
31	H	H	2,5-Dimethoxy
32	H	H	4-CH_3
33	H	H	3-F
34	H	H	4-F
35	H	H	3-Br
36	H	H	4-Br
37	H	H	4-Dimethyl amino
38	H	H	2,6-diCl
39	H	H	2,3-diCl
40	H	H	2,3-diCl
41	CH_3	H	2-Cl
42	CH_3	H	4-Cl
43	H	CH_3	4-NO_2
44	Phenyl	H	4-Cl

Table 1 (*Contd.*)

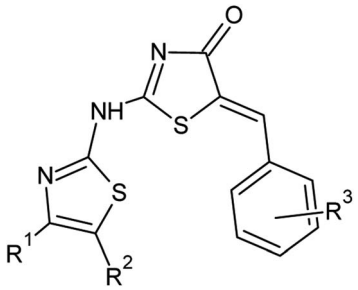

Compounds 28 to 47

Sl. no	R^1	R^2	R^3
45	Phenyl	H	2-Cl
46	Phenyl	H	3-Cl
47	Phenyl	H	4-Cl

Molecule	IUPAC name	Exp IC_{50} (nM)	pIC_{50}
1 (Training)	(2*E*)-1-[4-methyl-2-(methylamino)-1,3-thiazol-5-yl]-3-phenylprop-2-en-1-one	329.4	6.48
2 (Training)	(2*E*)-1-[4-methyl-2-(methylamino)-1,3-thiazol-5-yl]-3-(4-nitrophenyl) prop-2-en-1-one	247.5	6.61
3 (Training)	(2*E*)-1-[4-methyl-2-(methylamino)-1,3-thiazol-5-yl]-3-(3-nitrophenyl) prop-2-en-1-one	280.5	6.56
4(Test)	(2*E*)-3-(4-chlorophenyl)-1-[4-methyl-2-(methylamino)-1,3-thiazol-5-yl]prop-2-en-1-one	290.5	6.54
5 (Training)	(2*E*)-3-(3-chlorophenyl)-1-[4-methyl-2-(methylamino)-1,3-thiazol-5-yl]prop-2-en-1-one	290.5	6.54
6 (Training)	(2*E*)-3-(2-chlorophenyl)-1-[4-methyl-2-(methylamino)-1,3-thiazol-5-yl]prop-2-en-1-one	305.8	6.51
7 (Training)	(2*E*)-3-(4-methoxyphenyl)-1-[4-methyl-2-(methylamino)-1,3-thiazol-5-yl]prop-2-en-1-one	341.8	6.47
8 (Training)	(2*E*)-3-(2-methoxyphenyl)-1-[4-methyl-2-(methylamino)-1,3-thiazol-5-yl]prop-2-en-1-one	347.2	6.46
9 (Training)	(2*E*)-3-(2,6-dichlorophenyl)-1-[4-methyl-2-(methylamino)-1,3-thiazol-5-yl]prop-2-en-1-one	305.8	6.51
10 (Training)	(2*E*)-3-(2,4-dichlorophenyl)-1-[4-methyl-2-(methylamino)-1,3-thiazol-5-yl]prop-2-en-1-one	305.8	6.64
11 (Training)	(2*E*)-3-(4-fluorophenyl)-1-[4-methyl-2-(methylamino)-1,3-thiazol-5-yl]prop-2-en-1-one	54.3	7.27
12 (Training)	(2*E*)-3-(3-fluorophenyl)-1-[4-methyl-2-(methylamino)-1,3-thiazol-5-yl]prop-2-en-1-one	72.5	7.14
13(Test)	(2*E*)-3-(3-bromophenyl)-1-[4-methyl-2-(methylamino)-1,3-thiazol-5-yl]prop-2-en-1-one	59.3	7.23
14 (Training)	(2*E*)-1-[4-methyl-2-(methylamino)-1,3-thiazol-5-yl]-3-(3-methylphenyl)prop-2-en-1-one	73.5	7.13

Table 1 (*Contd.*)

Molecule	IUPAC name	Exp IC_{50} (nM)	pIC_{50}
15 (Training)	(2*E*)-3-(2,3-dichlorophenyl)-1-[4-methyl-2-(methylamino)-1,3-thiazol-5-yl]prop-2-en-1-one	61.2	7.21
16 (Training)	(2*E*)-1-[2-(ethylamino)-4-methyl-1,3-thiazol-5-yl]-3-phenylprop-2-en-1-one	36.8	7.43
17(Test)	(2*E*)-1-[2-(ethylamino)-4-methyl-1,3-thiazol-5-yl]-3-(4-nitrophenyl) prop-2-en-1-one	47.3	7.36
18 (Training)	(2*E*)-1-[2-(ethylamino)-4-methyl-1,3-thiazol-5-yl]-3-(3-nitrophenyl) prop-2-en-1-one	47.3	7.36
19 (Training)	(2*E*)-3-(4-chlorophenyl)-1-[2-(ethylamino)-4-methyl-1,3-thiazol-5-yl]prop-2-en-1-one	49.0	7.31
20 (Training)	(2*E*)-3-(3-chlorophenyl)-1-[2-(ethylamino)-4-methyl-1,3-thiazol-5-yl]prop-2-en-1-one	49.1	7.31
21 (Training)	(2*E*)-3-(2-chlorophenyl)-1-[2-(ethylamino)-4-methyl-1,3-thiazol-5-yl]prop-2-en-1-one	48.9	7.31
22 (Training)	(2*E*)-1-[2-(ethylamino)-4-methyl-1,3-thiazol-5-yl]-3-(4-fluorophenyl) prop-2-en-1-one	51.7	7.29
23 (Training)	(2*E*)-1-[2-(ethylamino)-4-methyl-1,3-thiazol-5-yl]-3-(3-fluorophenyl) prop-2-en-1-one	51.7	7.29
24 (Training)	(2*E*)-3-(3-bromophenyl)-1-[2-(ethylamino)-4-methyl-1,3-thiazol-5-yl]prop-2-en-1-one	57.1	7.24
25(Test)	(2*E*)-1-[2-(ethylamino)-4-methyl-1,3-thiazol-5-yl]-3-(4-methoxyphenyl)prop-2-en-1-one	49.7	7.3
26 (Training)	(2*E*)-1-[2-(ethylamino)-4-methyl-1,3-thiazol-5-yl]-3-(2-methoxyphenyl)prop-2-en-1-one	33.1	7.48
27 (Training)	*E*(2*E*)-1-[4-methyl-2-(propylamino)-1,3-thiazol-5-yl]-3-phenylprop-2-en-1-one	70.0	7.15
28(Test)	(5*Z*)-5-[(3-hydroxyphenyl) methylidene]-2-[(1,3-thiazol-2-yl) amino]-1,3-thiazol-4(5*H*)-one	110	6.96
29(Test)	(5*Z*)-5-[(4-hydroxy-3,5-dimethoxyphenyl)methylidene]-2-[(1,3-thiazol-2-yl)amino]-1,3-thiazol-4(5*H*)-one	31.3	7.5
30 (Training)	(5*Z*)-5-[(2-methoxyphenyl) methylidene]-2-[(1,3-thiazol-2-yl)amino]-1,3-thiazol-4(5*H*)-one	115	6.94
31 (Training)	(5*Z*)-5-[(2,5-dimethoxyphenyl) methylidene]-2-[(1,3-thiazol-2-yl)amino]-1,3-thiazol-4(5*H*)-one	33.0	7.48
32 (Training)	(5*Z*)-5-[(4-methylphenyl) methylidene]-2-[(1,3-thiazol-2-yl)amino]-1,3-thiazol-4(5*H*)-one	65.4	7.18
33 (Training)	(5*Z*)-5-[(3-fluorophenyl) methylidene]-2-[(1,3-thiazol-2-yl)amino]-1,3-thiazol-4(5*H*)-one	32.7	7.49

Table 1 (*Contd.*)

Molecule	IUPAC name	Exp IC_{50} (nM)	pIC_{50}
34 (Training)	(5*Z*)-5-[(4-fluorophenyl) methylidene]-2-[(1,3-thiazol-2-yl)amino]-1,3-thiazol-4(5*H*)-one	14.6	7.84
35(Test)	(5*Z*)-5-[(3-bromophenyl) methylidene]-2-[(1,3-thiazol-2-yl)amino]-1,3-thiazol-4(5*H*)-one	27.3	7.56
36 (Training)	(5*Z*)-5-[(4-bromophenyl) methylidene]-2-[(1,3-thiazol-2-yl)amino]-1,3-thiazol-4(5*H*)-one	15.2	7.81
37 (Training)	(5*Z*)-5-{[4-(dimethylamino)phenyl] methylidene}-2-[(1,3-thiazol-2-yl)amino]-1,3-thiazol-4(5*H*)-one	28.1	7.55
38 (Training)	(5*Z*)-5-[(2,6-dichlorophenyl) methylidene]-2-[(1,3-thiazol-2-yl)amino]-1,3-thiazol-4(5*H*)-one)	28.1	7.55
39 (Training)	(5Z)-5-[(2,3-dichlorophenyl) methylidene]-2-[(1,3-thiazol-2-yl)amino]-1,3-thiazol-4(5*H*)-one	28.1	7.55
40 (Training)	(5*Z*)-5-[(2,3-dichlorophenyl) methylidene]-2-[(1,3-thiazol-2-yl)amino]-1,3-thiazol-4(5*H*)-one	119.2	6.92
41 (Training)	(5*Z*)-5-[(2-chlorophenyl) methylidene]-2-[(4-methyl-1,3-thiazol-2-yl)amino]-1,3-thiazol-4(5*H*)-one	30.0	7.52
42 (Training)	((5*Z*)-5-[(4-chlorophenyl) methylidene]-2-[(4-methyl-1,3-thiazol-2-yl)amino]-1,3-thiazol-4(5*H*)-one	29.0	6.54
43 (Training)	(5*Z*)-2-[(5-methyl-1,3-thiazol-2-yl)amino]-5-[(4-nitrophenyl) methylidene]-1,3-thiazol-4(5*H*)-one	27.0	6.57
44(Test)	(5*Z*)-5-benzylidene-2-[(4-phenyl-1,3-thiazol-2-yl)amino]-1,3-thiazol-4(5*H*)-one	25.0	6.6
45 (Training)	(5*Z*)-5-[(2-chlorophenyl) methylidene]-2-[(4-phenyl-1,3-thiazol-2-yl)amino]-1,3-thiazol-4(5*H*)-one	25.2	6.59
46 (Training)	(5*Z*)-5-[(3-chlorophenyl) methylidene]-2-[(4-phenyl-1,3-thiazol-2-yl)amino]-1,3-thiazol-4(5*H*)-one	50.0	7.3
47 (Training)	(5*Z*)-5-[(4-chlorophenyl) methylidene]-2-[(4-phenyl-1,3-thiazol-2-yl)amino]-1,3-thiazol-4(5*H*)-one	17.0	7.77

dataset compounds were converted to their respective logarithmic values; pIC_{50} and numbering were reported for ease against literature reference papers.[62,63] Table 1 displays the dataset compounds along with their IC_{50} and pIC_{50} values.

Molecule structure preparation and 3D geometry optimization

Compound structures were drawn and subjected to the geometry optimization tool of Avogadro V1.2.0 by applying MMFF94,

molecular mechanics force field and steepest descent algorithm.[64] Various molecular formats were obtained from Open Babel V2.4.1 wherever necessary.[65] The best conformer for each dataset compound was obtained from Avogadro's genetic algorithm tool, using the 'energy' scoring function.

Data setup. The aforementioned molecules were subjected to PaDEL software and other descriptor calculation tools of Chemdes-Chemopy servers to calculate their respective values.[66] The variables were pre-filtered and organized by removing all-zero value, missing value and semi-constant or near constant value (>50%) descriptors. The pairwise correlation was utilized to filter out 786 descriptors with >0.85 value. A total of 38 variables having >0.40 cut-off correlation value were selected for the study. For compound selection, a cut-off value of 0.85 pairwise correlations was considered, from which 47 compounds were included in the study, partitioned into training and test sets in a 4 : 1 ratio based on the response order. Out of many models obtained from different trials, the best model follow-up procedure is discussed here.

Variable selection and model calculation. Various options in the QSARINS software explore the possible combinations of descriptors selected.[59–61] The genetic algorithm was employed for the structure bioactivity relationship and utilized for model fitness evaluation. A LOF smoothness level of 1.0, population size of 200, mutation probability of 0.1 and maximum generations of 5000 were chosen to explore more combinations.

Model validation. QSARINS models were subjected to validation criteria, both internal and external, along with applicability domain checking. Q^2_{LMO} was internally evaluated 5000 times with 30% of objects left randomly from the training set each time. The Y-scrambling procedure was set to 5000 iterations, which involve shuffling of the response data, to avoid chance correlation, meaning that the R^2 and Q^2loo values must be logically higher than the scrambled ones and the RMSE under prediction should be smaller than the scrambled ones. For predictivity of the models, various external validation parameters, implemented in QSARINS, were analyzed.[67] The leverage approach is represented by the subsequent Williams plot. The leverage or critical value (hat) was calculated by $h_i = x_i\,(X^T\,X)^{-1}\,x^T_i$ ($i = 1, 2, \ldots, m$), where x_i = the query compound's descriptor row-value and m = the number of query compounds. X was an $n*p$ matrix for the training set, where n = training set samples count and p = model descriptors count. The limit of model domain, h^* is $3\,(p+1)/n$, which was the leverage cut-off value. A leverage greater than h^* for the training set means that the compound is highly significant in model determination and in the test set (X outlier), the prediction will be model extrapolation. Compounds with a standardized residual greater than 2.5 σ (2.5 standard deviation units) were considered as Y outliers.

***In silico* ADMET studies.** The compounds with the best predicted model activity values were considered for *in silico* ADMET predictions using SWISS-ADME,[68] ADMESAR[69] and ProToxII[70] servers. The results are discussed in detail. Furthermore, docking studies were carried out for all the selected compounds.

Molecular docking studies. Autodock V4.2.6 was used to assess the affinities and interactions of DNA gyrase B inhibitors in conjunction with the created QSAR model.[71] The protein data bank provides the initial structure of the 3D structure of the DNA GyrB, pdb id: 6J90 (**https://w3.rcsb.org**). Missing residues were corrected using the Modeller V9.23 programme,[72] along with the addition of hydrogen atoms and the removal of preexisting ligands. To find docking parameters useful for docking-specified molecules, co-crystallized ligand to 6J90 redocking was carried out. All of the ligand structures were geometry optimized using Avogadro V1.2.0's steepest descent technique with a convergence parameter of 10×10^{-7} and the MMFF94 force field. Wherever necessary, file format conversions were made using Open Babel V2.4.1.

Proteins were created by geometrically adding polar hydrogens and assigning Kollman's united atom charges to create a pdbqt file. Along with the addition of polar hydrogens, the ligand is prepared by adding gasteiger charges. Torsions in the ligands were discovered, and a pdbqt file was created. The grid size was set to 60*60*60 points with a spacing of 0.375 Å and a distance-dependent function of the dielectric constant was used to calculate the energetic map. The autogrid option renders a selection of active sites. The grid box contains the enzyme's active binding site and has room for the ligand's rotational and translational movement.

For investigating ligand conformation poses and orientations inside the active site of DNA gyrase B, a Lamarckian evolutionary approach was employed. The following were the optimised parameters: the maximum number of energy assessments per run was increased to 25,000,000, the population size was set at 150, the maximum number of generations was 2700, and the gene mutation rate was set at 0.02. The default settings were used for all other variables. In a positional RMSD, results that varied by two points were grouped together. The representative of each group was the lowest binding energy configuration with the highest percentage frequency. The Discovery studio visualizer 2020 version 20.1.0.19295 (ref. 73) application created and displayed representations of ligand postures and interactions displayed.

Molecular dynamics simulations

Based on the Autodock binding energy of protein–ligand complexes, the best ligands from the designer dataset as well as reference compounds were identified and taken over for molecular dynamics simulations to study the physical changes in the atoms and molecules upon interacting with the solvent environment using the Desmond package of the Schrodinger 2021 molecular modelling suite.[74]

Results and discussion

Model information

The selected dataset molecules were optimized for geometry and by using MMFF94. ~3000 descriptors were calculated using PaDEL software, on the Chemopy-chemdes (RDKit and Bluedesc) server. The dataset was divided into training and test sets based on chemical and biological diversity. Several QSAR model equations were generated using QSARINS. Some of the models displayed higher R^2 and Q^2_{LOO} values, but their external

Table 2 The model 3 descriptor correlation matrix

	AATS8i	AVP-1	MoRSEE17	GATSe7
AATS8i	1.0000			
AVP-1	−0.1249	1.0000		
MoRSEE17	0.0949	0.0704	1.0000	
GATSe7	0.0330	0.3081	0.1359	1.0000

validation was not good along with too many outliers. Generally, the QSAR model should be cross validated to check its internal performance (robustness) and external performance given to be predictive capacity (predictability).

Model 1 developed with the aforementioned options gave optimal statistical values along with one outlier (compound 43 from training set) in the Williams plot at the 2.5 standard deviation unit level, and high 'RMSE' value and low Q^2_{LOO} and Q^2_{LMO} values. Subsequently, model 2 was generated and analyzed for outliers and betterment of the statistical values. Finally, the outliers (compounds 43, 33 and 27 from training set) were removed from the dataset and analyzed further for generating final validated model 3. The statistical parameters of models 1 and 2 are presented in ESI Table 1.†

Model 3:

$pIC_{50} = -9.1545 + 0.0798\ (AATS8i) + 10.0218\ (AVP\text{-}1) + 0.3957\ (MoRSEE17) + 0.5990\ (GATSe7)$.

$n_{tr} = 36$, $n_{pred} = 08$, $R^2 = 0.7065$, $R^2_{adj} = 0.6687$, $R^2 - R^2_{adj} = 0.0379$, LOF = 0.0894, $RMSE_{tr} = 0.2325$, $MAE_{tr} = 0.1873$, $RSS_{tr} = 1.9466$, $CCC_{tr} = 0.8280$, s = 0.2506, F = 18.6577, $Q^2_{LOO} = 0.6013$, $Q^2_{LMO} = 0.5701$, $R^2_{Yscr} = 0.1150$, $Q^2_{Yscr} = -0.1966$, $RMSE_{cv} = 0.2710$, $MAE_{cv} = 0.2182$, $PRESS_{cv} = 2.6444$, $CCC_{cv} = 0.7686$, $R^2_{ext} = 0.7540$, $MAE_{ext} = 0.1911$, $PRESS_{ext} = 0.3199$, $RMSE_{ext} = 0.200$, $CCC_{ext} = 0.8509$, $Q^2_{F1} = 0.7022$, $Q^2_{F2} = 0.7015$, $Q^2_{F3} = 0.7830$.

Model 3 showed good fitting criteria with validation values. Compared to previous models, model 3 showed better internal validation parameters with no outliers in the Williams plot. The model 3 descriptor correlation matrix is represented in Table 2. The scatter plot denotes the experimental *vs.* calculated inhibitory activities of chalcone derivatives and Fig. 1 displays predicted values similar to parallel experimental values. The K_{xy}, the inter-correlation among descriptors and response *vs.* Q^2_{LMO} of model 3 are plotted in ESI Fig. 1† showing the LMO parameter values around the model parameters, meaning that the model is robust and stable. ESI Fig. 2† displays the Y-scramble plot of K_{xy} *vs.* R^2_{Yscr} and Q^2_{Yscr}, which means that the correlation coefficients of model 3 are much greater than those after endpoint scrambling and a broken relationship can be noticed between the structure and responses. Standardized residuals *vs.* leverage values shown in Fig. 2 as the Williams plot illustrate the applicability domain of the model, by which one can depict whether the molecules are located in the applicability domain of the model or not. From the plot, the leverage values were found to be lower than the warning h^* of 0.417. The Q^2_{F1}, Q^2_{F2} and Q^2_{F3} values are near to the threshold value of 0.70. These results state that there is no chance correlation and truly there is a meaningful relationship between the chalcone derivatives with corresponding inhibitory activity. Model 3 containing molecular descriptors contributed structural information relating to the predicted bioactivity and the information obtained is compared to structure activity relationship studies of the dataset. The molecular descriptors contributing to model 3 were discussed in detail in ref. 75–77. Table 3 displays residual

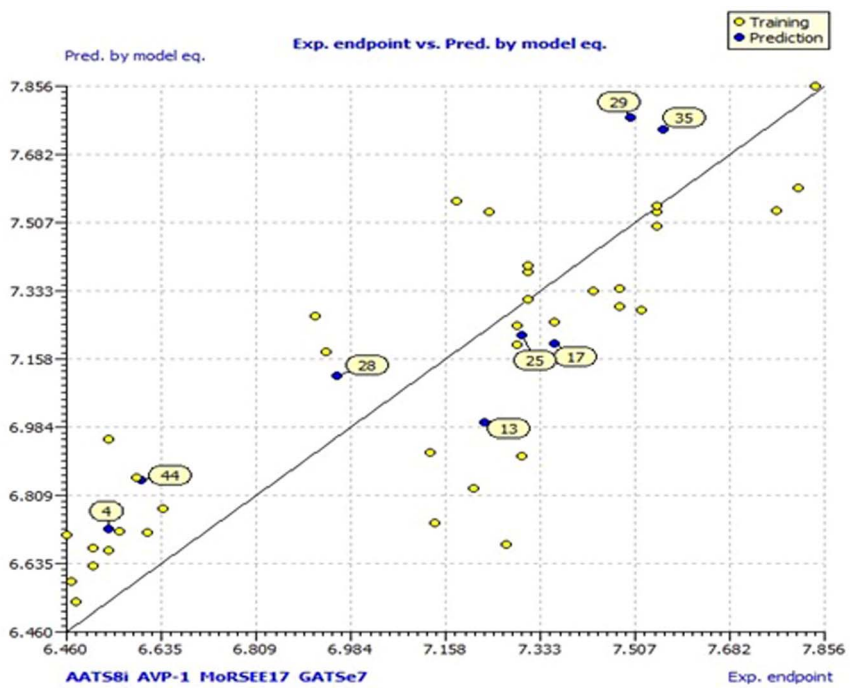

Fig. 1 Model 3 scatter plot.

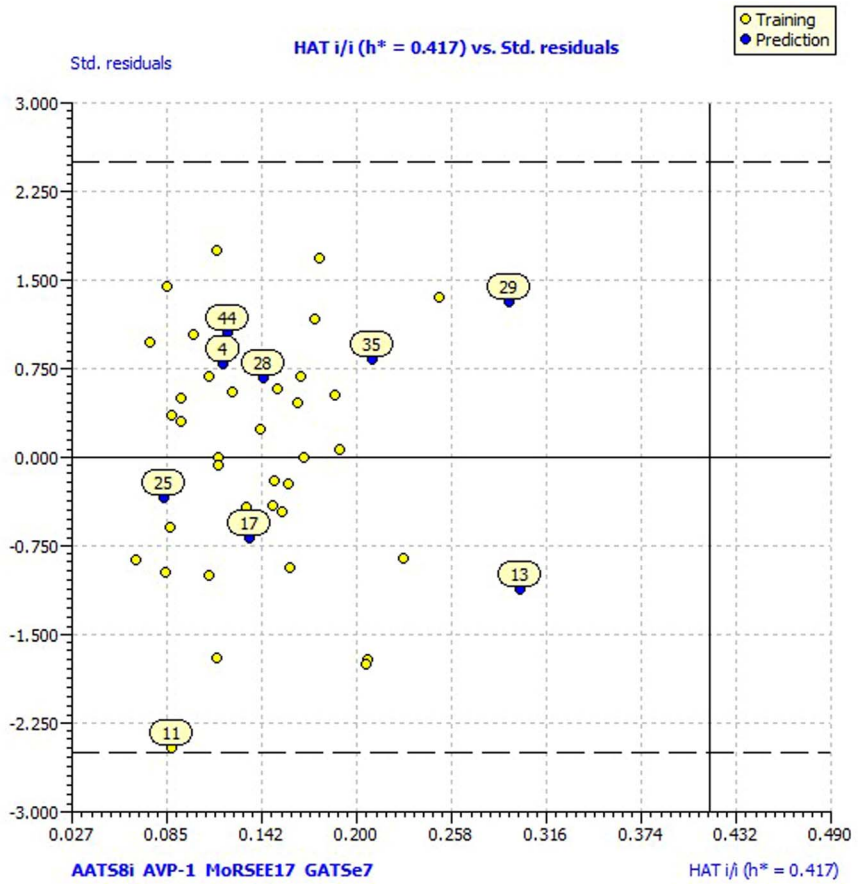

Fig. 2 Model 3 Williams plot.

information of compound bioactivity compared with the experimental *vs.* QSAR best model.

The molecular descriptors influencing the inhibitory activity are:

(i) AATS8i: This is the "averaged Moreau–Broto autocorrelation of lag 8 weighted by ionization potential". This descriptor positively affects the activity as per final model information.

(ii) AVP-1: This is "average valence path order 1", which is a topological descriptor that gives information regarding the connectivity of various atoms in the molecule and is referred to as a connectivity index calculated using the Chi operator. This descriptor depends on the number of lone pair and π electrons. According to the model, this descriptor positively affects the activity.

(iii) MoRSEE17: This is a 3D molecular representation of the structure based on electron diffraction data upon weightage of 17 value for Sanderson electronegativity.

(iv) GATSe7: This is "Geary coefficient of lag 1 weighted by Sanderson electronegativities". It negatively affects the activity.

SAR studies of the dataset

On analyzing the bioactivity results from the original dataset as shown in Table 1, compounds 1 to 27 having a thiazole ring attached to the chalcone have shown activity compared to the others. Similarly compounds 28 to 47 with substitutions on the R^1, R^2 and R^3 positions also have shown good inhibitory activity. Substitution with electron withdrawing groups at the R^2 position of the phenyl ring, such as nitro, decreases the activity, but substitution with fluorine at the ortho, meta and para positions increases the activity gradually. Di-substitution of halogens increases the activity on the phenyl ring. Substitution of methoxy, hydroxy and methyl groups on the phenyl ring also increases the activity. Substitution of heterocyclic groups drastically decreases the activity. Substitution of bulkier groups at the R^1 position increases the activity. Based on SAR studies of the original dataset and model equation parameters, two hundred compounds were designed and checked for predicted bioactivity using model 3. Table 4 displays the designed compounds' structural information and Table 5 displays the model predicted bioactivity of the designed compounds.

Study of the applicability domain of the QSAR model to the newly designed compounds

The designed compounds by SAR analysis predicted for pIC_{50} applying model 3 have been analyzed for their distribution in the chemical space of the original dataset defined by the model descriptors by applying a Principal Component Analysis (PCA).

The PCA loading plot of the original dataset with 44 molecules for model 3 descriptors is presented in ESI Fig. 3† having a Principal Component 1 (PC1) value of 37.20% and PC2 value

Table 3 pIC_{50} values of the dataset predicted by model 3 along with residuals

Compound	Exp pIC_{50}	Pred pIC_{50}	Residuals
1	6.4800	6.5367	0.0567
2	6.6100	6.7171	0.1071
3	6.5600	6.7181	0.1581
4 (Test)	6.5400	6.7263	0.1863
5	6.5400	6.6708	0.1308
6	6.5100	6.6745	0.1645
7	6.4700	6.5912	0.1212
8	6.4600	6.7083	0.2483
9	6.5100	6.6308	0.1208
10	6.6400	6.7761	0.1361
11	7.2700	6.6836	−0.5864
12	7.1400	6.7416	−0.3984
13 (Test)	7.2300	6.9963	−0.2337
14	7.1300	6.9212	−0.2088
15	7.2100	6.8289	−0.3811
16	7.4300	7.3348	−0.0952
17 (Test)	7.3600	7.2007	−0.1593
18	7.3600	7.2547	−0.1053
19	7.3100	7.3843	0.0743
20	7.3100	7.3115	0.0015
21	7.3100	7.3981	0.0881
22	7.2900	7.2469	−0.0431
23	7.2900	7.1971	−0.0929
24	7.2400	7.5364	0.2964
25 (Test)	7.3000	7.2208	−0.0792
26	7.4800	7.3396	−0.1404
27	7.1500	7.1012	−0.0487
28 (Test)	6.9600	7.1157	0.1557
29 (Test)	7.5000	7.7784	0.2784
30	6.9400	7.1773	0.2373
31	7.4800	7.2930	−0.1870
32	7.1800	7.5631	0.3831
33	7.4900	7.0890	−0.4002
34	7.8400	7.8563	0.0163
35 (Test)	7.5600	7.7473	0.1873
36	7.8100	7.5975	−0.2125
37	7.5500	7.4993	−0.0507
38	7.5500	7.5352	−0.0148
39	7.5500	7.5508	0.0008
40	6.9200	7.2694	0.3494
41	7.5200	7.2850	−0.2350
42	6.5400	6.9531	0.4131
43	6.5700	6.880	0.3103
44 (Test)	6.6000	6.8491	0.2491
45	6.5900	6.8574	0.2674
46	7.3000	6.9113	−0.3887
47	7.7700	7.5388	−0.2312

of 25.54%. The score plot of the original dataset with 44 molecules for model 3 presented in Fig. 3 showcases the chemical space ranging from the *X*-axis: −3.139 to 2.289 and *Y*-axis: −2.425 to 2.304 data points.

For a better understanding of the structural diversity of the designed compounds, the Williams plot and scatter plot are presented in Fig. 4 and 5, respectively. Fig. 4 envisages the h^* value of 0.076 notified using model 3 for all the compounds. C1 and C121 of the designer series were identified as X-outliers, distant from the applicability domain, and C63, C103, 31, 33, 34, 35 and 43 were identified as Y-outliers as explored by model

Table 4 Designer series molecules having chalcone and thiazole hybrid moieties

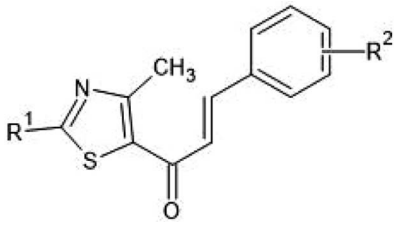

R^1	1–40	41–80	81–120	121–160	161–200
	$-CH_3$	$-C_2H_5$	$-C_3H_7$		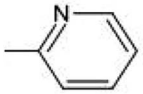

R^2

Sl. no	Group	Sl. no	Group	Sl. no	Group
1, 41, 81, 121, 161	2-OH	16, 56, 96, 136, 176	2-OH, 6-OH	31, 71, 111, 151, 191	2-CH_3, 6-CH_3
2, 42, 82, 122, 162	2-NO_2	17, 57, 97, 137, 177	2-OH, 5-CH_3	32, 72, 112, 152, 192	2-OCH_3, 3-OCH_3, 5-Br
3, 43, 83, 123, 163	2-F	18, 58, 98, 138, 178	3-CH_3, 4-OH	33, 73, 113, 153, 193	2-OCH_3, 3-OCH_3, 5-Cl
4, 44, 84, 124, 164	2-CF_3	19, 59, 99, 139, 179	2-OH, 3-CH_3	34, 74, 114, 154, 194	2-OCH_3, 6-OCH_3, 4- 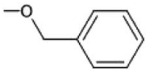
5, 45, 85, 125, 165	2-CH_3	20, 60, 100, 140, 180	2-OH, 4-OH, 6-CH_3	35, 75, 115, 155, 195	2-OCH_3, 4-OCH_3, 5-Br
6, 46, 86, 126, 166	2-OC_2H_5	21, 61, 101, 141, 181	2-CH_3, 4-OH	36, 76, 116, 156, 196	2-OCH_3, 4-OCH_3
7, 47, 87, 127, 167	3-OC_2H_5	22, 62, 102, 142, 182	2-OH, 3-CH_3, 5-F	37, 77, 117, 157, 197	3-OCH_3, 4-OCH_3
8, 48, 88, 128, 168	4-OC_2H_5	23, 63, 103, 143, 183	3-CH_3, 5-CH_3	38, 78, 118, 158, 198	2-OCH_3, 6-OCH_3
9, 49, 89, 129, 169	4-C_3H_7	24, 64, 104, 144, 184	3-CH_3, 4-OH, 5-CH_3	39, 79, 119, 159, 199	3-OCH_3, 5-OCH_3
10, 50, 90, 130, 170	4- 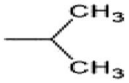	25, 65, 105, 145, 185	3-CH_3, 5-CH_3, 4- 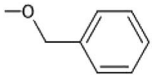	40, 80, 120, 160, 200	2-OCH_3, 3-OCH_3

Table 4 (*Contd.*)

R^2					
Sl. no	Group	Sl. no	Group	Sl. no	Group
11, 51, 91, 131, 171	4- 	26, 66, 106, 146, 186	2-OH, 3-CH_3, 5-CH_3		
12, 52, 92, 132, 172	4-C_2H_5	27, 67, 107, 147, 187	3-CH_3, 4-F, 5-CH_3		
13, 53, 93, 133, 173	2-OH, 3-OH	28, 68, 108, 148, 188	2-CH_3, 5-CH_3		
14, 54, 94, 134, 174	2-OH, 4-OH	29, 69, 109, 149, 189	2-OH, 3-CH_3, 4-CH_3		
15, 55, 95, 135, 175	2-OH, 5-OH	30, 70, 110, 150, 190	2-CH_3, 4-CH_3		

3. In Fig. 5, the scatter plot for all the dataset compounds and designed molecules shows 33 and C1, C121 distant from the regression line of model 3.

Similarly, the loading plot of both the designed and dataset compounds for the model 3 descriptors presented a PC1 value of 36.39% and PC2 value of 23.82% in ESI Fig. 4.† The score plots of both the designed and dataset compounds for model 3 presented in Fig. 6 showcase the chemical space ranging from the *X*-axis: −2.497 to 3.307 and *Y*-axis: −2.170 to 2.938 data points.

It is evident that the majority of designed molecules have been part of interpolation of the dataset and inside the structural applicability domain. The designed compounds having substitutions of 3-methyl, 3-methoxy or their combination at the R^2 position were found to be out of the applicability domain of the proposed model and therefore their predictions were extrapolated. The data predicted for these compounds are, at least, less reliable than those of the other compounds. It's noteworthy that 2-hydroxyl groups and compounds having a combination of groups at the R^2 position have shown excellent predicted activity as well as structural domain applicability (compounds C53 and C54, C93 and C94, C133 and C134, C173 and C174). In a similar case, the applicability region specified that a 5-Br group at the R^2 position is not beneficial (on comparing the pIC_{50} values of 35 and 36, 75 and 76, 115 and 116, 155 and 156, and 195 and 196). Overall, the applicability domain of the designed compounds projected that 2-hydroxyl, 2-nitro, 2-ethoxy and 2-methyl groups were beneficial at the R^2 position following methyl group, thiazole and pyridyl rings at the R^1 position. Model 3 was promising in this regard as the probability of accordance between the predicted and

Table 5 Model 3 predicted pIC_{50} values for the designed compounds

Compound	AATS8i	AVP-1	MoRSEE17	GATSe7	pIC_{50}
C1	154.6222	0.329386	−1.458	0.965	6.126499
C2	156.3947	0.354614	0.873	0.759	7.319758
C3	155.1452	0.341639	0.53	1.03	7.116621
C4	155.3775	0.350394	0.719	0.709	7.105405
C5	158.4803	0.340196	0.971	0.829	7.422403
C6	157.8188	0.362151	0.985	1.138	7.780273
C7	158.1324	0.353156	1.432	0.769	7.67099
C8	158.0306	0.344036	1.29	0.814	7.542242
C9	157.5324	0.353156	1.278	0.826	7.596317
C10	159.1588	0.351713	1.194	0.826	7.678412
C11	155.4385	0.362411	0.899	0.79	7.350451
C12	157.4171	0.353405	0.962	0.842	7.474156
C13	153.281	0.327647	0.523	0.88	6.735005
C14	155.3199	0.362411	0.629	0.932	7.319209
C15	153.0582	0.362671	0.545	0.88	7.076943
C16	157.2212	0.363802	0.525	0.998	7.483249
C17	157.5538	0.347839	0.81	1.155	7.556633
C18	160.0419	0.330409	0.937	1.06	7.573848
C19	160.1868	0.363802	0.65	1.155	7.86341
C20	160.6462	0.342408	0.778	0.875	7.568591
C21	158.208	0.342408	0.844	0.798	7.354022
C22	160.2244	0.342648	0.456	0.94	7.448853
C23	161.0717	0.342169	1.08	1.568	8.134755
C24	156.0422	0.353276	1.255	1.244	7.719884
C25	157.7357	0.342648	1.732	0.912	7.738393
C26	151.5597	0.338894	1.088	1.326	7.201085
C27	152.0352	0.329295	1.239	1.065	7.046242
C28	154.5617	0.337509	0.855	1.18	7.247114
C29	154.1035	0.323774	0.917	1.138	7.072279
C30	149.674	0.349949	1.203	0.816	6.901419
C31	154.5698	0.34995	1.538	0.793	7.410891
C32	155.1016	0.349728	1.231	0.999	7.453021
C33	152.1663	0.349728	1.174	0.944	7.163285
C34	152.3011	0.363089	1.696	1.23	7.68581
C35	155.3243	0.320381	0.955	1.045	7.095017
C36	153.74	0.358745	0.745	1.042	7.268184
C37	151.1758	0.335595	1.036	0.776	6.787358
C38	155.4989	0.366629	1.338	1.226	7.83242
C39	152.2192	0.331254	0.898	0.737	6.749158
C40	152.2154	0.331024	1.238	0.993	7.034434
C41	152.2192	0.331024	1.067	1.155	7.064107
C42	151.4043	0.331254	1.461	0.885	6.995564
C43	152.5082	0.341655	1.031	1.142	7.171673
C44	153.2633	0.341655	1.355	0.753	7.12713
C45	152.5082	0.341885	1.225	1.18	7.273507
C46	155.3194	0.320096	1.48	1.312	7.459452
C47	150.25	0.334196	1.581	0.973	7.033128
C48	150.3495	0.341655	1.52	1.024	7.122228
C49	153.9338	0.332914	1.736	1.192	7.506753
C50	153.4696	0.352055	1.635	1.192	7.621577
C51	153.9632	0.344433	1.228	1.153	7.400165
C52	155.8359	0.338089	1.505	1.208	7.628591
C53	153.2788	0.344433	0.757	1.007	7.071725
C54	155.0042	0.343151	0.739	1.06	7.221181
C55	150.7438	0.352285	0.881	1.007	6.99719
C56	153.1473	0.344655	1.187	1.116	7.298892
C57	155.3243	0.320096	1.238	1.326	7.372464
C58	152.1195	0.354211	1.135	1.244	7.368744
C59	148.0179	0.352515	1.177	1.326	7.090184
C60	153.0541	0.35458	0.906	1.003	7.212046
C61	153.4321	0.340268	0.796	1	7.053457
C62	158.1649	0.325888	1.065	1.022	7.406644
C63	156.8756	0.35458	1.428	1.857	8.235106

Table 5 (*Contd.*)

Compound	AATS8i	AVP-1	MoRSEE17	GATSe7	pIC_{50}
C64	157.3901	0.335149	1.476	1.411	7.833266
C65	154.1755	0.335149	1.935	1.07	7.554108
C66	156.9177	0.335362	1.182	1.483	7.724505
C67	157.8667	0.334935	1.422	1.176	7.70702
C68	154.2766	0.320381	1.189	1.493	7.37236
C69	153.6387	0.335362	1.209	1.312	7.371095
C70	153.3833	0.311854	1.343	1.166	7.080681
C71	153.7329	0.304529	1.398	1.129	7.034779
C72	155.9892	0.310522	1.659	1.108	7.365585
C73	155.4626	0.300053	1.319	1.041	7.043977
C74	151.6464	0.322485	2.021	1.301	7.397769
C75	155.677	0.324447	1.521	1.154	7.453169
C76	156.1458	0.324233	1.344	1.161	7.422593
C77	153.6774	0.324233	1.493	0.915	7.13722
C78	153.7141	0.337117	1.516	1.328	7.525756
C79	155.4186	0.333257	1.509	0.874	7.348385
C80	154.9298	0.332928	1.643	1.111	7.501063
C81	152.6653	0.313728	1.568	1.081	7.080285
C82	154.5577	0.331084	1.784	0.836	7.343959
C83	153.8906	0.305499	1.182	1.071	6.93687
C84	153.8874	0.305278	1.551	0.717	6.868359
C85	153.8906	0.305278	1.434	1.108	7.056528
C86	153.1922	0.305499	1.6	1.242	7.148966
C87	154.041	0.315514	1.826	0.918	7.212425
C88	154.6947	0.315514	1.754	0.962	7.262457
C89	154.041	0.315736	1.927	1.121	7.376208
C90	156.3708	0.333257	1.734	1.121	7.661352
C91	152.033	0.309256	1.462	1.095	6.951449
C92	152.1723	0.315514	1.855	1.132	7.202965
C93	155.2751	0.308019	0.906	0.948	6.889715
C94	154.7942	0.32553	1.034	0.993	7.104429
C95	155.1906	0.319127	1.187	0.948	7.105486
C96	156.3913	0.318583	1.097	1.051	7.22193
C97	154.5906	0.319127	1.602	1.252	7.403919
C98	156.1342	0.31789	1.265	1.169	7.331638
C99	152.4139	0.325751	1.55	1.252	7.276025
C100	154.4753	0.319341	1.309	0.947	7.098224
C101	155.4186	0.333542	1.507	0.94	7.389982
C102	152.2953	0.325751	1.003	0.97	6.881198
C103	150.0336	0.325973	1.837	1.758	7.504959
C104	154.3579	0.330622	1.512	1.337	7.515857
C105	154.6906	0.316788	2.309	1.043	7.54302
C106	158.5296	0.30773	1.548	1.41	7.677302
C107	157.6303	0.330622	1.659	1.115	7.702183
C108	158.0897	0.311035	1.712	1.413	7.742015
C109	155.3448	0.311035	1.291	1.242	7.253953
C110	157.6679	0.311242	1.285	1.099	7.353377
C111	158.5152	0.310829	1.635	1.069	7.537376
C112	155.0877	0.31847	1.672	1.056	7.347296
C113	152.4747	0.324485	1.562	0.993	7.117799
C114	154.8724	0.311242	1.476	1.272	7.3095
C115	152.6969	0.333257	2.35	1.097	7.597547
C116	157.2161	0.322912	1.476	1.1	7.510455
C117	156.3779	0.346134	1.462	0.864	7.529397
C118	156.8736	0.337049	1.457	1.267	7.717314
C119	157.4161	0.331617	1.661	0.828	7.523929
C120	156.0313	0.337049	1.577	1.056	7.571195
C121	158.2808	0.335475	−1.46	0.97	6.481681
C122	152.9979	0.346419	0.808	0.782	6.954621
C123	155.8694	0.337321	0.839	0.971	7.218061
C124	158.7334	0.327655	0.561	0.68	7.065426
C125	152.8296	0.346419	0.973	0.954	7.109505
C126	149.6179	0.346704	0.95	1.119	6.945804

Table 5 (*Contd.*)

Compound	AATS8i	AVP-1	MoRSEE17	GATSe7	pIC_{50}
C127	155.6547	0.349925	1.182	0.83	7.378509
C128	156.1167	0.332632	1.271	0.863	7.297051
C129	159.8323	0.317914	1.052	0.962	7.418706
C130	159.8327	0.349925	1.35	0.962	7.857454
C131	160.4451	0.326067	0.726	0.942	7.408336
C132	157.0253	0.326067	1	0.969	7.260031
C133	159.8828	0.326327	0.614	0.874	7.281018
C134	161.0124	0.325807	0.282	0.909	7.255543
C135	157.5813	0.31222	0.638	0.874	6.965482
C136	156.3693	0.326327	0.637	0.966	7.064848
C137	160.1081	0.340399	1.029	1.127	7.755786
C138	160.2586	0.329	0.647	1.048	7.455079
C139	163.2627	0.33875	0.684	1.127	7.854488
C140	161.943	0.322572	0.356	0.874	7.305694
C141	157.7387	0.353561	0.789	0.848	7.436524
C142	161.1574	0.353247	0.341	0.904	7.562462
C143	161.6664	0.352987	0.994	1.498	8.214671
C144	159.4841	0.352987	0.917	1.202	7.832754
C145	159.1825	0.368672	1.33	0.963	7.986136
C146	151.9438	0.343206	0.554	1.273	7.031901
C147	160.2699	0.363573	1.247	1.019	8.022507
C148	157.814	0.336277	1.05	1.213	7.591227
C149	160.3564	0.362702	1.313	1.119	8.106705
C150	160.4329	0.331303	1.146	1.094	7.717072
C151	160.4293	0.331031	1.066	0.928	7.582972
C152	160.4329	0.331031	1.044	0.988	7.610491
C153	159.6609	0.331303	0.628	0.932	7.353459
C154	160.1691	0.343594	1.375	1.217	7.983493
C155	160.8871	0.343594	1.269	1.021	7.881442
C156	160.1691	0.343866	0.754	1.013	7.618292
C157	157.4539	0.343819	0.984	0.796	7.362178
C158	157.7753	0.334754	0.937	1.048	7.429325
C159	158.1166	0.343594	0.878	0.768	7.35409
C160	161.5245	0.333249	1.025	0.978	7.706323
C161	160.6147	0.355885	0.743	0.987	7.75438
C162	160.8729	0.346771	1.212	0.789	7.750623
C163	159.4946	0.339005	0.906	0.97	7.550146
C164	160.2191	0.346771	0.879	0.672	7.496606
C165	162.0784	0.345266	0.913	1.019	7.851196
C166	158.0147	0.356157	0.983	1.135	7.733245
C167	160.0935	0.347031	1.144	0.86	7.70666
C168	158.1017	0.343547	1.181	0.892	7.546605
C169	157.8852	0.356157	1.442	1.033	7.843439
C170	155.4147	0.356429	0.982	1.033	7.466996
C171	159.8031	0.358354	0.878	1.021	7.788141
C172	160.1646	0.341753	1.533	1.037	7.919384
C173	161.4762	0.32527	0.42	0.878	7.323211
C174	162.6989	0.358354	0.547	0.91	7.821762
C175	163.1936	0.335842	0.542	0.878	7.614478
C176	160.8757	0.335842	0.743	0.965	7.561161
C177	162.7394	0.336091	0.878	1.14	7.870625
C178	163.6518	0.335593	0.975	1.064	7.931297
C179	154.8149	0.343547	1.075	1.14	7.390926
C180	160.3623	0.336091	0.594	0.88	7.412812
C181	156.9037	0.347654	0.794	0.875	7.328842
C182	157.1416	0.336125	0.489	0.899	7.125976
C183	159.6289	0.34608	0.99	1.542	8.007633
C184	158.7664	0.329669	0.98	1.215	7.574506
C185	154.9502	0.360217	0.789	0.999	7.37116
C186	158.5026	0.359362	1.022	1.283	7.908383
C187	158.9714	0.359112	1.269	1.023	7.885294
C188	156.7452	0.359112	0.882	1.269	7.701861
C189	156.6161	0.374144	0.637	1.135	7.664984

Table 5 (*Contd.*)

Compound	AATS8i	AVP-1	MoRSEE17	GATSe7	pIC_{50}
C190	154.7802	0.359945	1.385	1.015	7.600291
C191	157.7187	0.369257	1.318	0.995	7.889613
C192	155.4542	0.342124	1.256	0.988	7.408255
C193	157.5823	0.368672	1.228	0.93	7.798315
C194	157.2993	0.338637	1.867	1.219	7.900692
C195	157.2961	0.338377	0.651	1.019	7.296857
C196	157.2993	0.338377	1.231	1.014	7.523625
C197	156.6009	0.338637	1.143	0.808	7.312281
C198	157.2462	0.350394	1.257	1.169	7.742952
C199	157.8999	0.350394	0.897	0.781	7.420255
C200	157.2462	0.350654	1.215	0.982	7.616927

actual values is as high as that for the training set compounds (Table 3).

In silico ADMET studies

The twelve compounds with >7.9 pIC_{50} values listed in ESI Tables 2 and 3† were studied for their ADMET properties using SWISSADME, ADMESAR & Protox Studies. The key outcomes are listed below:

(1) According to SWISS ADME studies all of the selected 12 compounds pass the Lipinski rule of five.

(2) All the compounds have molar refractivity in the range of 40–130.

(3) All the compounds have a total polar surface area in the range of 20–130.

(4) Lipophilicity log P is less than 5.

(5) Out of the 12 compounds, 9 are moderately soluble, and 7 have high intestinal absorption.

(6) None of the compounds was a PGP substrate, so the intestinal efflux is low, and a small dose will be sufficient for drug activity.

(7) All compounds were CYP450 enzyme inhibitors, so first pass metabolism will be less and even with a low dose the bioavailability will be high.

The intestinal absorption of the molecule upon oral administration is given by the HIA score and was found to be between 0.956 and 0.1 for the best designed compounds, indicating that the compounds were well absorbed from the intestines. The predicted cell permeability Caco2 lies in the range of (0.50–0.801), which helps in better intestinal absorption and is also found to be in the acceptable range (−1 to +1). The designed compounds show a blood–brain barrier probability score of (0.9715–0.979), which implies that they cross the blood–brain barrier, producing an effect on CNS activity.

The best designed compounds are devoid of toxicological endpoints; for example, the carcinogenicity binary, immunotoxicity and cytotoxicity are within acceptable ranges, which was

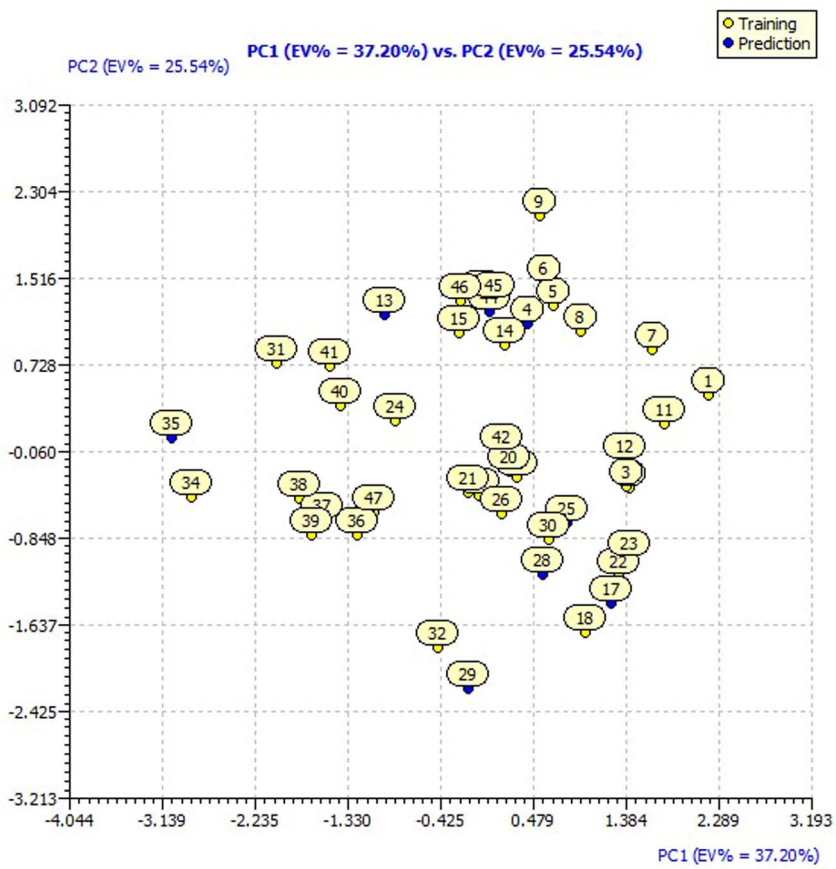

Fig. 3 PCA score plot of model 3 with compound names.

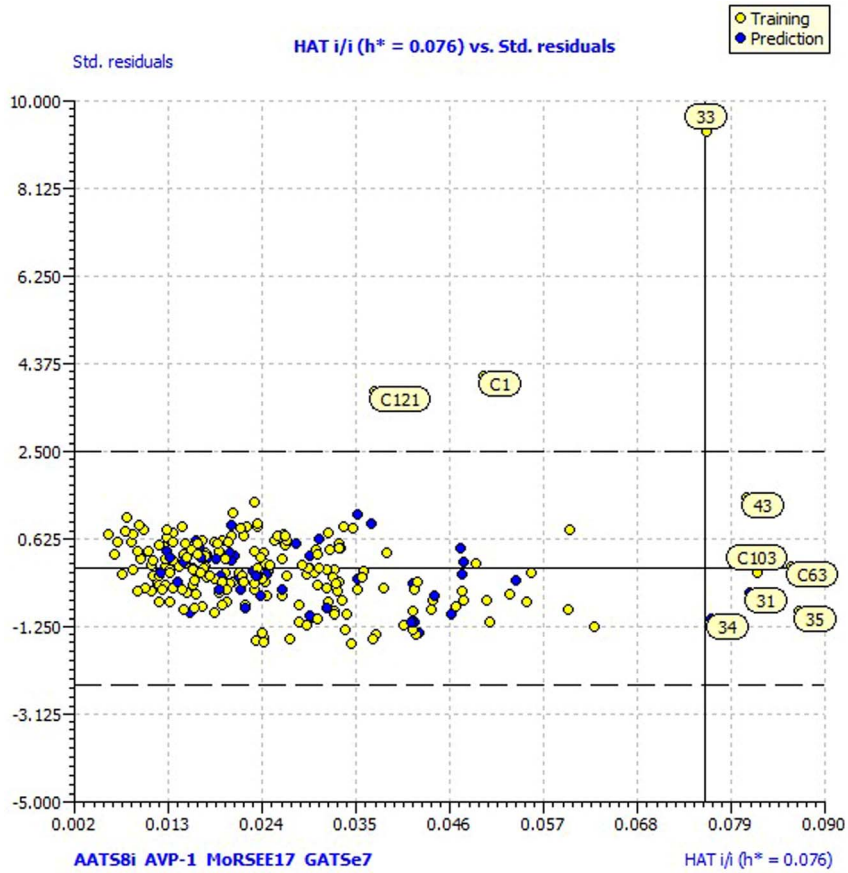

Fig. 4 Williams plot of the designed and dataset compounds.

identified by using Protox-II. The acute oral toxicity values reveal that all 12 compounds comes under class IV drugs of toxicity, showing LD_{50} values in the range of (300–2000 mg kg^{-1}). The solubility values range from −3.303 to 4.775, and the more negative the value, the higher the solubility up to −10. All 12 compounds have shown high plasma binding protein capacity, which in-turn influences the drug biological half-life. The bound portion acts as a reservoir from which the drug will be slowly released as unbound form, and then the unbound form is metabolized and excreted rapidly. ESI Tables 1 and 2 detail† the ADMET results from various servers.

Molecular docking studies

H-bond interactions were seen in compound 143 with the residues Cys268, Gln275 and Ile266 of the 6J90 protein. Compound 143 with a thiazole group at the R^1 position interacted with Gln275 and Ile266 by hydrogen bonding followed by the nitrogen of the ligand thiazole ring with Cys268. The best active site conformation from Autodock results in a binding affinity of compound 143 with 6J90 protein of −9.7 kcal mol^{-1}. Similarly, H-bond interactions were predicted in compound 145 with residues Gln335, Tyr26, His38 and Lys103 of the 6J90 protein. Compound 145 display H-bonds near to the R^1 position with Tyr26, followed by oxygen of chalcone interaction with Gln335. His38 interacted with the thiazole N atom forming a favorable H-bond. The oxygen atom on the methoxy phenyl group of compound 145 interacted well with Lys103. The best active site conformation from Autodock results in a binding affinity of compound 145 with the 6J90 protein of −10.47 kcal mol^{-1}.

Again, H-bond interactions were seen in compound 172 with the residues Cys268 and Gln275 of the 6J90 protein. Compound 172 with a pyridyl group at the R^1 position does not show any interactions, followed by H-bonding of the amino group near the thiazole ring interacting with Cys268 and Gln275. The best active site conformation from Autodock results in the binding affinity of compound 172 with the 6J90 protein of −8.79 kcal mol^{-1}. Similarly, H-bond interactions were predicted in compound 178 with the residues Cys268, Ile266, Arg276 and Lys189 of the 6J90 protein. Compound 178 displays H-bonds near to the amine group of the thiazole ring R^1 position with Lys189. The oxygen of the chalcone interacted with the amine group of Arg276, and the hydroxyl group interacted with Cys268 and Ile266. The best active site conformation from Autodock results in the binding affinity of compound 17 with the 3ZKD protein of −8.65 kcal mol^{-1}.

With various substituents at the R^1 and R^2 positions, the designed series gave a few best leads based on predicted values using QSAR model 3. These leads were evaluated for H-bond interactions and binding scores using molecular docking

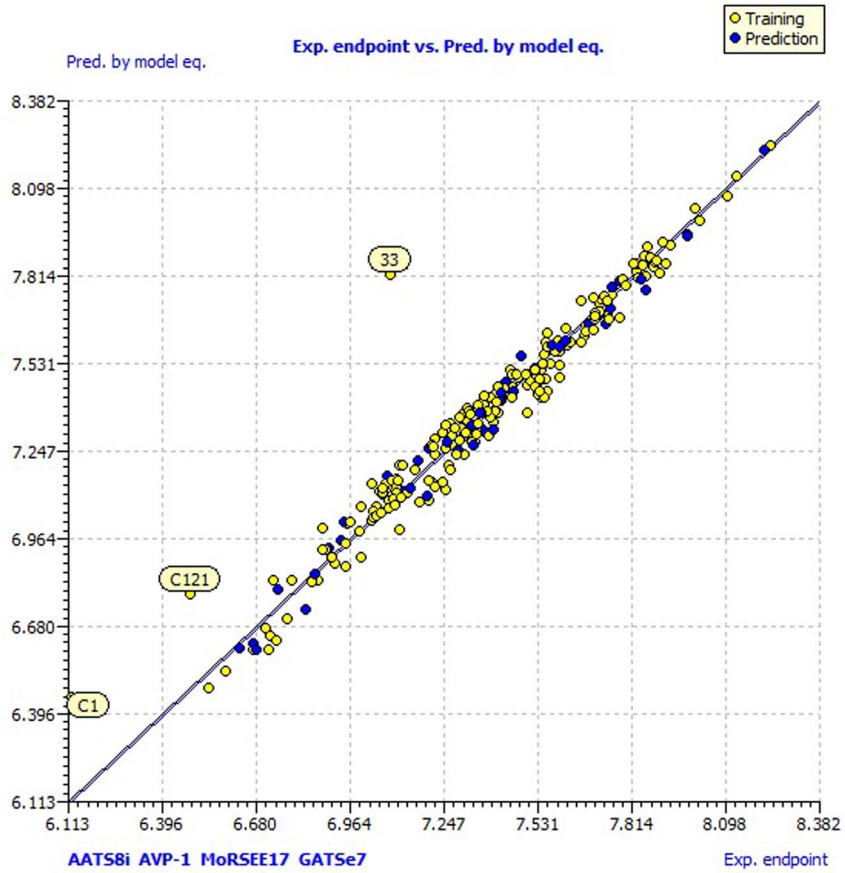

Fig. 5 Scatter plot of the designed and dataset compounds.

studies. The results are presented in Table 4 with interacting residues, and binding affinity scores from Autodock. The results are favorable giving importance to model equation descriptors supporting QSAR studies. In general, the molecular descriptors (weighted or unweighted) of the obtained QSAR model and type of molecular docking interactions (charged, hydrogen bond, dipole–dipole, van der Waals, pi-cation, *etc.*), were correlated and found to be in association with each other. ESI Fig. 5a–d† (5a-ligand 143, 5b-ligand 145, 5c-ligand 172, and 5d-ligand 178) show the docking interactions of the best compounds with 6J90 from Discovery studio visualizer 2020. To confirm the interactions and stability in the active site of DNA gyrase B, compounds 143, 145, 172 and 178 of the designed compounds were taken over for molecular dynamics simulations using the DESMOND package.

Molecular dynamics simulations

Compounds 143, 145, 172 and 178, and reference compound vosaroxin, were subjected to molecular dynamics simulations to analyze the stability of the ligands in the active-site cavity. However, it was observed that compounds 143 and 145 show fluctuations in their conformations during the simulation time (ESI Fig. 6d and 7d†). This clearly denotes instability of the ligands and furthermore, the RMSD graph of compound 172 showed fluctuations leading to an unsteady graph (ESI Fig. 8a†). Thus, compound 172 in the 6J90 active-site cannot be considered as best-fit. Analyzing further, compound 178 in the active-site of 6J90 has shown good stability, with no fluctuations in the H-bond network with the residues.

DNA gyrase 6J90 with compound 178: detailed investigation. The backbone structure and C-alpha residues were analyzed from the simulation data. The ligand fit protein in Fig. 7a displayed fluctuations up to 10 nanoseconds (0.6–2.6 Å) and displayed incremental stability until 100 nanoseconds. The RMSD average value of the protein backbone is 2.4 Å, which lies within the standard limit (<3 Å) and for the protein-reference complex, the average and maximum value was found to be 2.403 Å and 2.971 Å at 22 nanoseconds.

Dynamic properties of the protein. The RMSF graph indicates that there are no local changes along the protein chain during the thermal motion. The fluctuations are seen mildly in helices and moderately in loops. The 'N' and 'C' end terminals fluctuated higher than the other regions in the protein. The more rigid secondary structure elements like α-helices and β-strands are less fluctuated compared to the loop region residues, which participated in 70% of the simulation time (Fig. 7b).

H-bond analysis. The complex conformation displayed water bridges, 'H' bonds, hydrophobic contacts and ionic

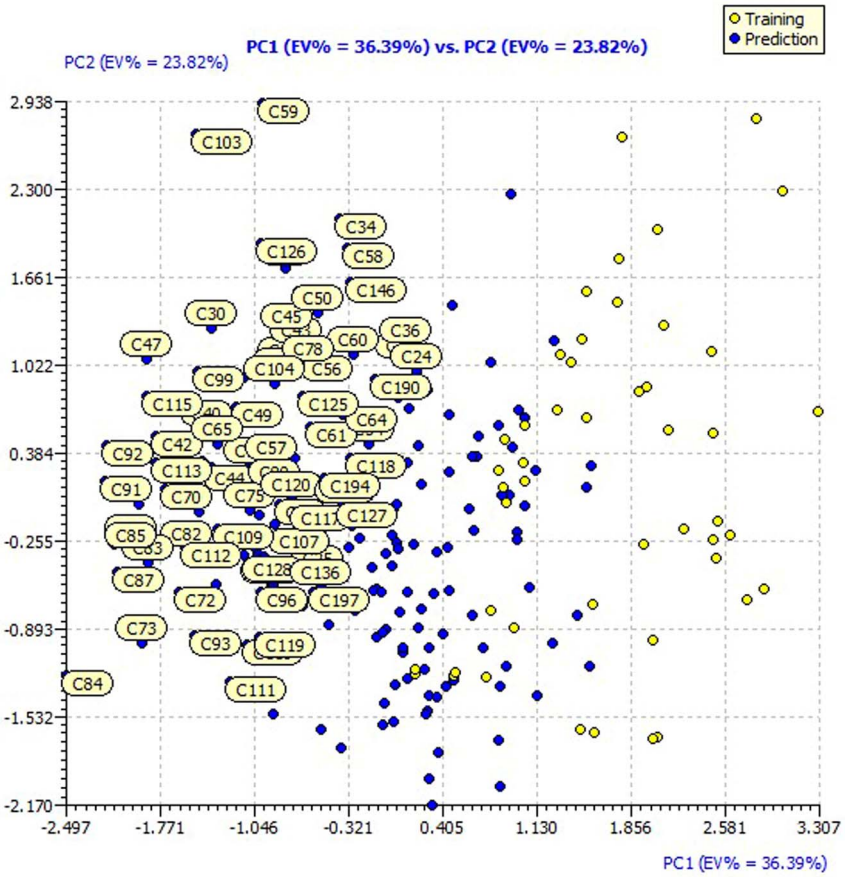

Fig. 6 PCA score plot of the designed and dataset compounds.

interactions. There are four H-bond interactions at residues Asn46, Asp73, Gly77 and Gly119 at the maximum of 99% of the simulation time. The residues Asp43 interact with the hydroxyl group on the phenyl ring, exhibiting a H-bond of about 99% of the simulation time. The residues Gly102, Val118 and His116 showed H-bond interactions with water bridges towards the chalcone oxygen, amine bridge and pyridyl nitrogen. Lys103 have shown H-bonds along with a water-bridge and hydrophobic interactions with the amine-bridge. All these vital residues play a key role for ligand binding and stabilization of the reference molecule complex (Fig. 7c).

Percentage residue of H-bond analysis. The 'H' bond analysis in the protein ligand contact denotes aromatic stacking interactions of the thiazole nitrogen with Gly119 for 7% simulation time. The other residues Asp73 and Gly77 showed 99% and 96% interaction during the simulation run with the hydroxyl group of the phenyl ring, respectively. His116 has shown interaction along the water-bridge for 37% of the simulation time with the pyridyl nitrogen. Similarly, Gly117 has shown interaction along the water-bridge for 41% of the simulation time with the pyridyl nitrogen. It was noticed that Gly102 has shown direct interaction with the chalcone oxygen for 73% of the simulation time. From ESI Fig. 9c† and the interactions, it is clear that 'H' bonding along with additional water bridges favors the molecular stability throughout the simulation time.

Ligand properties

Radius of gyration (RoG) determines the compactness of the protein during simulation. The maximum and the average values for the ROG are 4.811 Å and 4.432 Å. The solvent exposed surface area determines the changes in conformation in terms of MolSA, SASA, and PSA. The average and the minimum values of MolSA were 340.23 Å and 345.22 Å. The minimum and the average value of the solvent accessible surface area is 1.296 Å and 10.98 Å, respectively. The PSA determines the polarity induced by electronegative atoms, and the minimum and average value of PSA is 112.16 Å and 124.92 Å (Fig. 7d).

DNA gyrase 6J90 with the reference compound. The ligand fit protein in ESI Fig. 9a† displayed fluctuations and displayed incremental stability occasionally until 100 nanoseconds. The RMSD average value of the protein backbone is 1.9 Å, which lies within the standard limit (<3 Å) and for the protein-reference complex, the average and maximum value were found to be 1.912 Å and 3.012 Å at 11 nanoseconds.

Dynamic properties of the protein. Fluctuations are seen in the helices and heavily in the loops. The more rigid secondary structure elements like α-helices and β-strands fluctuated less compared to the loop region residues, which participated in 90% of the simulation time (ESI Fig. 9b†).

Percentage residue of H-bond analysis. The 'H' bond analysis in the protein ligand contact denotes aromatic stacking

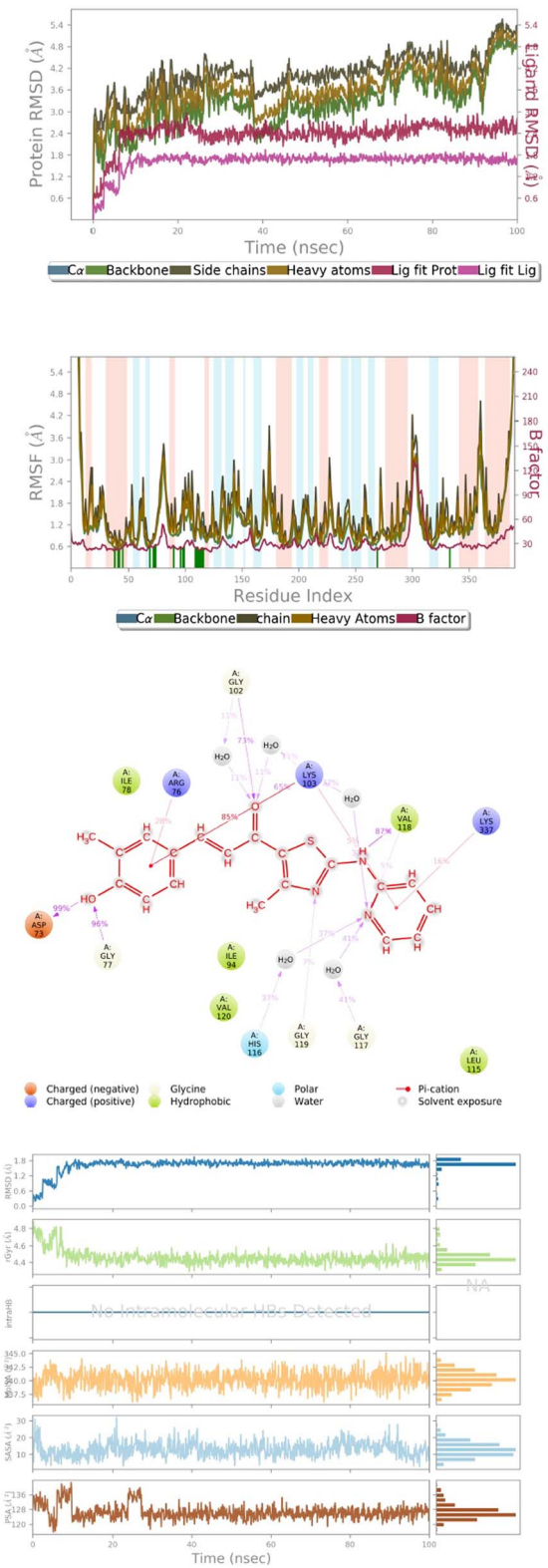

Fig. 7 (a) RMSD graph of ligand 178 with 6j90. (b) RMSF graph of ligand 178 with 6j90. (c) H-bond contacts of ligand 178 with 6j90. (d) Surface analysis of ligand 178 with 6j90.

interactions of the thiazole ring with Lys103 for 28% of the simulation time. The other residues, Thr165, Asp73 and Val43, showed 6%, 61% and 9% interaction during the simulation run with the methyl-amine substituent, respectively. Tyr109 showed interaction for 19% of the simulation time with the nitrogen-containing ring system. Similarly, Ser108 has shown interaction for 7% of the simulation time with a carboxylic acid group. From ESI Fig. 9c† and the interactions, it is clear that 'H' bonding along with the additional water bridges favors the molecular stability throughout the simulation time.

Ligand properties

The maximum and the average values for the Radius of Gyration are 4.256 Å and 4.392 Å. The average and the minimum values of MolSA were 352.12 Å and 341.56 Å. The minimum and the average value of solvent accessible surface area is 41.2 Å and 18.2 Å, respectively. The PSA determines the polarity induced by electronegative atoms, and the minimum and average value of PSA is 159.02 Å and 172.4 Å (ESI Fig. 9d†).

Estimation of the binding free energy of the compound 178_6J90 complex. The molecular mechanics-generalized born surface area (MM-GBSA) analysis's calculation of Gibbs free energy reveals a high correlation between the anticipated and experimental binding affinities. The OPLS forcefield-based molecular mechanics energies with the variable dielectric generalised born 2.0 (VSGB) solvation model, which takes into account residue-dependent effects, was used for the polar solvation term. Solvent-Accessible Surface Area (SASA), a nonpolar solvation term, was included in the Prime MM-GBSA approach along with van der Waals interactions to estimate the binding free energy (ΔG_{bind}) of the finished docked complex. The OPLS-2005 force field was used to optimise the docked conformations. In Prime MM-GBSA, the binding free energy of the 5FL4 protein and ligand complex was measured (molecular mechanics generalised born surface area). The Schrodinger suite's Prime module and the OPLS-2005 force field were used to compute the binding free energies of the receptor–ligand complexes. Using the free energy difference between the complex and the sum of the individual free energies of the protein and ligand, the binding free energy was computed.

$$\Delta G\ (\text{binding}) = \Delta G\ (\text{complex}) - \Delta G\ (\text{protein}) - \Delta G\ (\text{ligand})$$

where the binding free energy is denoted by ΔG (binding) and the free energy of the complex, protein, and ligand was denoted by ΔG (complex), ΔG (protein) and ΔG (ligand), respectively (Table 6).

Using the MMGBSA method and the MM-PBSA.py tool, binding free energies were calculated using 250 snapshots taken at evenly spaced intervals over the last 20 ns of the simulation. The H-bond interactions between the optimised lead molecules and the residues Arg76, Lys103, Lys337, Asp73, Val118, and His116 were demonstrated to remain constant. The RMSD increment of the ligand 178 according to Desmond calculations suggests a new binding mode, which was

Table 6 Docking interactions of the designed compounds

Compound no	Docking score (kcal mol^{-1})	Residue interactions and hydrogen bond distance in Å
23	−7.85	Arg276 (1.9 Å), Arg276 (2.3 Å)
63	−7.79	Arg276 (1.9 Å)
143	−9.7	Cys268 (2.0 Å), Gln275 (1.9 Å), Ile266 (1.8 Å)
145	−10.47	Gln335 (1.9 Å), Tyr26 (2.6 Å), His38 (2.1 Å), Lys103 (2.1 Å)
147	−8.2	Lys337 (2.73 Å)
149	−8.03	Arg276 (2.0 Å), His38 (2.2 Å), Asp45 (3.1 Å)
154	−8.78	Lys337 (2.2 Å), Gln335 (2.2 Å), Met25 (2.0 Å)
172	−8.79	Cys268 (1.8 Å), Gln275 (2.0 Å)
178	−8.65	Cys268 (2.1 Å), Ile266 (1.8 Å), Arg276 (2.0 Å) Arg276 (2.2 Å), Lys189 (1.9 Å)
183	−7.46	Cys268 (1.9 Å), Cys268 (2.2 Å)
186	−8.47	Arg276 (2.79 Å), His38 (2.9 Å)
194	−8.57	Ile186 (2.0 Å), Arg276 (2.1 Å), Glu193 (1.9 Å)

Table 7 The binding free energy details of the complex 6J90_compound 178

Energy component	Average	Std. deviation	Std. error of mean
Generalized born			
Van der Waals	−41.4585	2.6789	0.267
EEL	−8.1254	2.8745	0.287
EGB	−16.4589	1.8956	0.189
ESURF	−7.9966	0.2565	0.256
ΔG_{gas}	−49.5839	2.8978	0.289
ΔG_{solv}	−24.4555	1.5236	0.152
ΔG_{total}	−74.0394	1.6523	0.165
Poisson Boltzmann			
Van der Waals	−41.4585	2.6789	0.266
EEL	−8.1254	2.8745	0.287
EPB	−18.3599	1.9856	0.198
ENPOLAR	−5.1616	0.2689	0.268
EDISPER	0.0000	0.0000	0.000
ΔG_{gas}	−49.5839	2.9923	0.299
ΔG_{solv}	−23.5215	1.6895	0.168
ΔG_{total}	−73.1054	1.9875	0.198

subsequently investigated to see if it had any impact on the binding energy using the MM-PBSA (Poisson Boltzmann surface analysis) and the MMGBSA calculations. Table 7 lists the binding free energies for the complex 6J90 compound 178 in MM-GBSA and MM-PBSA. Van der Waals (−41.4585 kcal mol^{-1}) favoured the complex interactions more than electrostatic interactions in both techniques (−8.1254 kcal mol^{-1}). The polar solvation energy was found to be advantageous in the development of protein-inhibitor complexes (−16.4589 kcal mol^{-1} in MM-GBSA and −18.3599 kcal mol^{-1} in MM-PBSA). When compared to the complex stability achieved by MM-PBSA, the net binding energy for the complex anticipated by MM-GBSA was −74.0394 kcal mol^{-1} (−73.1054 kcal mol^{-1}). The new kind of conformation pose in binding can be more energetically beneficial, as seen by the increased binding energy in MM-GBSA. It was discovered that the net energy disparities between the MM-PBSA and MM-GBSA approaches were reliable.

Conclusion

The current study focused on performing QSAR analysis of 47 chalcone derivatives utilizing validation criteria of the QSARINS software. The molecular descriptors utilized to develop the validated model favored designing compounds based on dataset structure–activity relationship information. The applicability domain of the designed 200 compounds was explored in the QSAR model region and the leads were obtained. Further ADMET profiles for the compounds with the best predicted bioactivity were analyzed and molecular docking studies were performed for active-site analysis. The stability of lead compounds 143, 145, 172 and 178 was determined using molecular dynamics simulations and upon analysis, compound 178 emerged as the best lead candidate, which can be explored further. The binding free energy decomposition analysis further indicates that residues Lys103, Asp73, Arg76, Lys337, Val118 and His116 are essential for the high selectivity of DNA gyrase B inhibition. Overall, these results serve as a significant guideline for the discovery and design of novel DNA gyrase B inhibitors.

Conflicts of interest

There are no conflicts to declare.

Acknowledgements

The authors are thankful to the Research Council of GITAM and VISTAS, and the QSARINS software license provider Dr Gramatica P.

References

1 A. Ayati, S. Emami, A. Asadipour, A. Shafiee and A. Foroumadi, Recent applications of 1,3-thiazole core structure in the identification of new lead compounds and drug discovery, *Eur. J. Med. Chem.*, 2015, **5**, 699–718.
2 T. M. Chhabria, S. Patel, P. Modi and S. P. Brahmkshatriya, Thiazole: a review on chemistry, synthesis and therapeutic importance of its derivatives, *Curr. Top. Med. Chem.*, 2016, **16**, 2841–2862.

3 Z. Chunlin, Z. Wen, S. Chunquan, Z. Wannian, X. Chengguo and M. Zhenyuan, Chalcone: a Privileged Structure in Medicinal Chemistry, *Chem. Rev.*, 2017, **117**, 7762–7810.

4 K. S. Yazdan, G. V. Sagar and B. A. Shaik, Biological and synthetic potentiality of chalcones: a review, *J. Chem. Pharm. Res.*, 2015, **7**, 829–842.

5 T. I. De Santana, B. M. De Oliveira, G. P. A. De Moraes, A. C. Da Cruz, T. G. Da Silva and A. C. Leite, Synthesis, anticancer activity and mechanism of action of new thiazole derivatives, *Eur. J. Med. Chem.*, 2018, **20**, 874–886.

6 S. M. Gomha, M. M. Edrees and F. M. A. Altalbawy, Synthesis and Characterization of Some New Bis-Pyrazolyl-Thiazoles Incorporating the Thiophene Moiety as Potent Anti-Tumor Agents, *Int. J. Mol. Sci.*, 2016, **17**, 1499.

7 P. Takac, M. Kello, M. Vilkova, J. Vaskova, R. Michalkova, G. Mojzisova and J. Mojzis, Antiproliferative Effect of Acridine Chalcone is Mediated by Induction of Oxidative Stress, *Biomolecules*, 2020, **10**, 345.

8 S. M. Gomha, S. A. Ahmed and A. O. Abdelhamid, Synthesis and Cytotoxicity Evaluation of Some Novel Thiazoles, Thiadiazoles, and Pyrido [2,3-*d*] [1,2,4] triazole [4,3 – *a*] pyrimidin – 5(1*H*)- ones Incorporating Triazole Moiety, *Molecules*, 2015, **20**, 1357–1376.

9 S. Patel, R. Patle, P. Parameswaran, A. Jain and A. Shard, Design, computational studies, synthesis and biological evaluation of thiazole – based molecules as anticancer agents, *Eur. J. Pharm. Sci.*, 2019, **134**, 20–30.

10 S. Abu-Melha, M. M. Edrees, H. H. Salem, N. A. Kheder, S. M. Gomha and M. R. Abdelaziz, Synthesis and biological evaluation of some novel thiazole-based heterocycles as potential anticancer and antimicrobial agents, *Molecules*, 2019, **24**, 539.

11 T. A. Farghaly, G. S. Masaret, Z. A. Muhammad and M. F. Harras, Discovery of thiazole based chalcones and 4-hetarylthiazoles as potent anticancer agents: synthesis, docking study and anticancer activity, *Bioorg. Chem.*, 2020, **98**, 103761.

12 M. D. Altıntop, B. Sever, Ç. G. Akalın and A. Özdemir, Design, synthesis, and evaluation of a new series of thiazole-based anticancer agents as potent Akt inhibitors, *Molecules*, 2018, **23**, 1318.

13 V. Spanò, A. Attanzio, S. Cascioferro, A. Carbone, A. Montalbano, P. Barraja, L. Tesoriere, G. Cirrincione, P. Diana and B. Parrino, Synthesis and Antitumor Activity of New Thiazole Nortopsentin Analogs, *Mar. Drugs*, 2016, **14**, 226.

14 A. B. Shaik, R. R. Bhandare, S. Nissankararao, B. V. Lokesh, S. Shahanaaz and M. M. Rahman, Synthesis, and biological screening of chloropyrazine conjugated benzothiazepine derivatives as potential antimicrobial, antitubercular and cytotoxic agents, *Arabian J. Chem.*, 2021, **14**, 102915.

15 Y. Wang, W. Zhang, J. Dong and J. Gao, Design, synthesis and bioactivity evaluation of coumarin–chalcone hybrids as potential anticancer agents, *Bioorg. Chem.*, 2020, **95**, 103530.

16 A. Shaik, R. R. Bhandare, K. Palleapati, S. Nissankararao, V. Kancharlapalli and S. Shaik, Antimicrobial, Antioxidant, and Anticancer Activities of Some Novel Isoxazole Ring Containing Chalcone and Dihydropyrazole Derivatives, *Molecules*, 2020, **25**, 1047.

17 S. Madhavi, R. Sreenivasulu, J. P. Yazala and R. R. Raju, Synthesis of chalcone incorporated quinazoline derivatives as anticancer agents, *Saudi Pharm. J.*, 2017, **25**, 275–279.

18 H. R. M. Rashdan, A. H. Abdelmonsef, I. A. Shehadi, S. M. Gomha, A. M. M. Soliman and H. K. Mahmoud, Synthesis, Molecular Docking Screening and Anti-Proliferative Potency Evaluation of Some New Imidazo[2,1-*b*]Thiazole Linked Thiadiazole Conjugates, *Molecules*, 2020, **25**, 4997.

19 S. Madhavi, R. Sreenivasulu, A. M. Yousuf, A. M. Jawed and R. R. Ramesh, Synthesis, biological evaluation and molecular docking studies of pyridine incorporated chalcone derivatives as anticancer agents, *Lett. Org. Chem.*, 2016, **13**, 682–692.

20 Y. K. Abhale, A. Shinde, K. K. Deshmukh, L. Nawale, D. Sarkar and P. C. Mhaske, Synthesis, antitubercular and antimicrobial potential of some new thiazole substituted thiosemicarbazide derivatives, *Med. Chem. Res.*, 2017, **26**, 2557–2567.

21 S. T. Dhumal, A. R. Deshmukh, M. R. Bhosle, V. M. Khedkar, L. U. Nawale, D. Sarkar and R. A. Mane, Synthesis and antitubercular activity of new 1,3,4-oxadiazoles bearing pyridyl and thiazolyl scaffolds, *Bioorg. Med. Chem. Lett.*, 2016, **26**, 3646–3651.

22 N. U. Güzeldemirci, B. Karaman and Ö. Küçükbasmaci, Antibacterial, antitubercular and antiviral activity evaluations of some arylidene hydrazide derivatives bearing imidazo [2,1-*b*] thiazole moiety, *Turk. J. Pharm. Sci.*, 2017, **14**, 157.

23 M. Yan, L. Xu, Y. Wang, J. Wan, T. Liu, W. Liu, Y. Wan, B. Zhang, R. Wang and Q. Li, Opportunities and challenges of using five-membered ring compounds as promising antitubercular agents, *Drug Dev. Res.*, 2020, **81**, 402–418.

24 A. Kryshchyshyn, O. Roman, A. Lozynskyi and R. Lesyk, Thiopyrano [2,3-*d*]Thiazoles as New Efficient Scaffolds in Medicinal Chemistry, *Sci. Pharm.*, 2018, **86**, 26.

25 G. B. Gundlewad and B. R. Patil, Synthesis and Evaluation of Some Novel 2-Amino-4-Aryl Thiazoles for Antitubercular Activity, *J. Heterocycl. Chem.*, 2018, **55**, 769–774.

26 A. B. Shaik, R. R. Bhandare, S. Nissankararao, Z. Edis, N. R. Tangirala, S. Shahanaaz and M. M. Rahman, Design, facile synthesis and characterization of dichloro substituted chalcones and dihydropyrazole derivatives for their antifungal, antitubercular and antiproliferative activities, *Molecules*, 2020, **25**, 3188.

27 S. Pola, K. K. Banoth, M. Sankaranarayanan, R. Ummani and A. Garlapati, Design, synthesis, in silico studies, and evaluation of novel chalcones and their pyrazoline derivatives for antibacterial and antitubercular activities, *Med. Chem. Res.*, 2020, **29**, 1819–1835.

28 S. Burmaoglu, O. Algul, A. Gobek, A. D. Aktas, M. Ulger, B. G. Erturk, E. Kaplan, A. Dogen and G. Aslan, Design of potent fluoro – substituted chalcones as antimicrobial agents, *J. Enzyme Inhib. Med. Chem.*, 2017, **32**, 490–495.

29 A.-M. Borcea, I. Ionut, O. Cris and O. Oniga, An Overview of the Synthesis and Antimicrobial, Antiprotozoal, and Antitumor Activity of Thiazole and Bisthiazole Derivatives, *Molecules*, 2021, **26**, 624.

30 P. Kishor, K. V. Ramana and A. B. Shaik, Antitubercular evaluation of isoxazolyl chalcones, *Res. J. Pharm., Biol. Chem. Sci.*, 2017, **8**, 730–735.

31 B. V. Lokesh, Y. R. Prasad and A. B. Shaik, Synthesis and biological activity of novel 2,5-dichloro-3-acetylthiophene chalcone derivatives, *Indian J. Pharm. Educ. Res.*, 2017, **51**, 679–690.

32 A. M. Asiri and S. A. Khan, Synthesis and Anti-Bacterial Activities of a Bis-Chalcone Derived from Thiophene and Its Bis-Cyclized Products, *Molecules*, 2011, **16**, 523–531.

33 A. J. Kadhim, J. H. Mohammed and N. M. Aljamali, Thiazole Amide Derivatives (Synthesis, Spectral Investigation, Chemical Properties, Antifungal Assay), *NeuroQuantology*, 2020, **18**, 16.

34 M. Kucerova-Chlupacova, V. Vyskovska-Tyllova, L. Richterova-Finkova, J. Kunes, V. Buchta, M. Vejsova, P. Paterova, L. Semelkova, O. Jandourek and V. Opletalova, Novel Halogenated Pyrazine-Based Chalcones as Potential Antimicrobial Drugs, *Molecules*, 2016, **21**, 1421.

35 A. B. Shaik, R. P. Yejella and S. Shaik, Synthesis, Antimicrobial, and Computational Evaluation of Novel Isobutylchalcones as Antimicrobial Agents, *Int. J. Med. Chem.*, 2017, **2017**, 6873924.

36 G. Singh, A. Arora, P. Kalra, I. K. Maurya, C. E. Ruizc, M. A. Estebanc, S. Sinha, K. Goyal and R. Sehgal, A strategic approach to the synthesis of ferrocene appended chalcone linked triazole allied organo silatranes: antibacterial, antifungal, antiparasitic and antioxidant studies, *Bioorg. Med. Chem.*, 2019, **27**, 188–195.

37 A. B. Shaik, S. V. Lohitha, S. B. Puttagunta, A. Shaik, K. Supraja and H. K. Sai, Synthesis and screening of novel lipophilic diarylpropeones as prospective antitubercular, antibacterial and antifungal agents, *Biointerface Res. Appl. Chem.*, 2019, **9**, 3912–3918.

38 M. Mellado, L. Espinoza, A. Madrid, J. Mella, E. Chávez-Weisser, K. Diaz and M. Cuellar, Design, synthesis, antifungal activity, and structure–activity relationship studies of chalcones and hybrid dihydrochromane–chalcones, *Mol. Diversity*, 2019, **3**, 1–3.

39 S. B. Lagu, P. Y. Rajendra, N. Srinath and B. S. Afzal, Synthesis, antibacterial, antifungal antitubercular activities and molecular docking studies of nitrophenyl derivatives, *Int. J. Life Sci. Pharma Res.*, 2019, **9**, 54–64.

40 M. Djukic, M. Fesatidou, I. Xenikakis, A. Geronikaki, V. T. Angelova, V. Savic, M. Pasic, B. Krilovic, D. Djukic, B. Gobeljic, *et al.*, In vitro antioxidant activity of thiazolidinone derivatives of 1,3-thiazole and 1,3,4-thiadiazole, *Chem.-Biol. Interact.*, 2018, **286**, 119–131.

41 V. A. Adole, R. A. More, B. S. Jagdale, T. B. Pawar and S. S. Chobe, Efficient synthesis, antibacterial, antifungal, antioxidant and cytotoxicity study of 2-(2-hydrazineyl) thiazole derivatives, *ChemistrySelect*, 2020, **5**, 2778–2786.

42 C. Nastasa, B. Tiperciuc, M. Duma, D. Benedec and O. Oniga, New hydrazones bearing thiazole scaffold: synthesis, characterization, antimicrobial, and antioxidant investigation, *Molecules*, 2015, **20**, 17325–17338.

43 E. Polo, N. Ibarra-Arellano, L. Prent-Peñaloza, A. Morales-Bayuelo, J. Henao, A. Galdámez and M. Gutiérrez, Ultrasound-assisted synthesis of novel chalcone, heterochalcone and bis-chalcone derivatives and the evaluation of their antioxidant properties and as acetylcholinesterase inhibitors, *Bioorg. Chem.*, 2019, **90**, 103034.

44 J. Wang, L. Huang, C. Cheng, G. Li, J. Xie, M. Shen, Q. Chen, W. Li, W. He, P. Qiu, *et al.*, Design, synthesis and biological evaluation of chalcone analogues with novel dual antioxidant mechanisms as potential anti-ischemic stroke agents, *Acta Pharm. Sin. B*, 2019, **9**, 335–350.

45 N. A. Al Zahrani, R. M. El-Shishtawy, M. M. Elaasser and A. M. Asiri, Synthesis of Novel Chalcone-Based Phenothiazine Derivatives as Antioxidant and Anticancer Agents, *Molecules*, 2020, **25**, 4566.

46 N. Sun, Y. J. Lu, F. Y. Chan, R. L. Du, Y. Y. Zheng, K. Zhang, L. Y. So, R. Abagyan, C. Zhuo, Y. C. Leung, *et al.*, A thiazole orange derivative targeting the bacterial protein FtsZ shows potent antibacterial activity, *Front. Microbiol.*, 2017, **8**, 855.

47 E. Abdel-Latif, A. S. Almatari and G. E. Abd-ElGhani, Synthesis and Antibacterial Evaluation of Some New Thiazole-Based Polyheterocyclic Ring Systems, *J. Heterocycl. Chem.*, 2019, **56**, 1978–1985.

48 S. R. Vegesna, Y. R. Prasad and B. S. Afzal, Antimicrobial evaluation of some novel pyrazine based chalcones, *Int. J. Adv. Pharm. Sci.*, 2017, **8**, 11–18.

49 A. Özdemir, M. D. Altıntop, B. Sever, H. K. Gençer, H. A. Kapkaç, Ö. Atlı and M. Baysal, A New Series of Pyrrole-Based Chalcones: Synthesis and Evaluation of Antimicrobial Activity, Cytotoxicity, and Genotoxicity, *Molecules*, 2017, **22**, 2112.

50 X. Tang, S. Su, M. Chen, J. He, R. Xia, T. Guo, Y. Chen, C. Zhang, J. Wang and W. Xue, Novel chalcone derivatives containing a 1,2,4-triazine moiety: design, synthesis, antibacterial and antiviral activities, *RSC Adv.*, 2019, **9**, 6011–6020.

51 S. B. Lagu, R. P. Yejella, R. R. Bhandare and A. B. Shaik, Design, Synthesis, and Antibacterial and Antifungal Activities of Novel Trifluoromethyl and Trifluoromethoxy Substituted Chalcone Derivatives, *Pharmaceuticals*, 2020, **13**, 375.

52 P. V. Reddy, M. Hridhay, K. Nikhil, S. Khan, P. N. Jha, K. Shah and D. Kumar, Synthesis and investigations into the anticancer and antibacterial activity studies of β-carboline chalcones and their bromide salts, *Bioorg. Med. Chem. Lett.*, 2018, **28**, 1278–1282.

53 S. A. Khan and A. M. Asiri, Green synthesis, characterization and biological evaluation of novel chalcones as antibacterial agents, *Arabian J. Chem.*, 2017, **10**, S2890–S2895.

54 M. Zhang, A. M. Prior, M. M. Maddox, W. J. Shen, K. E. Hevener, D. F. Bruhn, R. B. Lee, A. P. Singh, J. Reinicke, C. J. Simmons, *et al.*, Pharmacophore modeling, synthesis, and antibacterial evaluation of

chalcones and derivatives, *ACS Omega*, 2018, **3**, 18343–18360.

55 A. Gomtsyan, Heterocycles in drugs and drug discovery, *Chem. Heterocycl. Compd.*, 2012, **48**, 7–10.

56 C. Viegas-Junior, A. Danuello, V. da Silva Bolzani, E. J. Barreiro and C. A. M. Fraga, Molecular hybridization: a useful tool in the design of new drug prototypes, *Curr. Med. Chem.*, 2007, **14**, 1829–1852.

57 K. V. Sashidhara, K. B. Rao, P. Kushwaha, R. K. Modukuri, P. Singh, I. Soni, P. K. Shukla, S. Chopra and M. Pasupuleti, Novel chalcone–thiazole hybrids as potent inhibitors of drug resistant Staphylococcus aureus, *ACS Med. Chem. Lett.*, 2015, **6**, 809–813.

58 S. Sinha, S. L. Manju and M. Doble, Chalcone–Thiazole Hybrids: Rational Design, Synthesis, and Lead Identification against 5-Lipoxygenase, *ACS Med. Chem. Lett.*, 2019, **10**, 1415–1422.

59 P. Gramatica, N. Chirico, E. Papa, S. Cassani and S. Kovarich, QSARINS: a new software for the development, analysis, and validation of QSAR MLR models, *J. Comput. Chem.*, 2013, **34**, 2121–2132, DOI: **10.1002/jcc.23361**.

60 P. Gramatica, Principles of QSAR Modeling: Comments and Suggestions from Personal Experience, *Int. J. Quant. Struct.-Prop. Relat.*, 2020, **5**(3), 61–97, DOI: **10.4018/IJQSPR.20200701.oa1**.

61 P. Gramatica, N. Chirico and S. Cassani, QSARINS-chem: Insubria datasets and new QSAR/QSPR models for environmental pollutants in QSARINS, *J. Comput. Chem.*, 2014, **35**, 1036–1044, DOI: **10.1002/jcc.23576**.

62 K. Liaras, A. Geronikaki, J. Glamočlija, A. Ćirić and M. Soković, Thiazole-based chalcones as potent antimicrobial agents. Synthesis and biological evaluation, *Bioorg. Med. Chem.*, 2011, **19**(10), 3135–3140.

63 C. Tratrat, M. Haroun, E. Tsolaki, A. Petrou, A. Gavalas and A. Geronikaki, Thiazole-based Chalcone Derivatives as Potential Anti-inflammatory Agents: Biological Evaluation and Molecular Modelling, *Curr. Top. Med. Chem.*, 2021, **21**(4), 257–268, DOI: **10.2174/1568026621999201214232458**.

64 M. D. Hanwell, D. E. Curtis, D. C. Lonie, *et al.*, Avogadro: an advanced semantic chemical editor, visualization and analysis platform, *J. Cheminf.*, 2012, **4**, 17, DOI: **10.1186/1758-2946-4-17**.

65 N. M. O'Boyle, M. Banck, C. A. James, *et al.*, Open Babel: an open chemical toolbox, *J. Cheminf.*, 2011, **3**, 33, DOI: **10.1186/1758-2946-3-33**.

66 J. Dong, D. S. Cao, H. Y. Miao, *et al.*, ChemDes: an integrated web-based platform for molecular descriptor and fingerprint computation, *J. Cheminf.*, 2015, **7**, 60, DOI: **10.1186/s13321-015-0109-z**.

67 P. Gramatica and A. Sangion, A Historical Excursus on the Statistical Validation Parameters for QSAR Models: A Clarification Concerning Metrics and Terminology, *J. Chem. Inf. Model.*, 2016, **56**(6), 1127–1131, DOI: **10.1021/acs.jcim.6b00088**.

68 A. Daina, O. Michielin and V. Zoete, SwissADME: a free web tool to evaluate pharmacokinetics, drug-likeness and medicinal chemistry friendliness of small molecules, *Sci. Rep.*, 2017, **7**, 42717, DOI: **10.1038/srep42717**.

69 F. Cheng, W. Li, Y. Zhou, J. Shen, Z. Wu, G. Liu, P. W. Lee and Y. Tang, admetSAR: A Comprehensive Source and Free Tool for Assessment of Chemical ADMET Properties, *J. Chem. Inf. Model.*, 2012, **52**(11), 3099–3105, DOI: **10.1021/ci300367a**.

70 P. Banerjee, A. O. Eckert, A. K. Schrey and R. Preissner, ProTox-II: a webserver for the prediction of toxicity of chemicals, *Nucleic Acids Res.*, 2018, **46**(W1), W257–W263, DOI: **10.1093/nar/gky318**.

71 J. Eberhardt, D. Santos-Martins, A. F. Tillack and S. Forli, AutoDock Vina 1.2.0: New Docking Methods, Expanded Force Field, and Python Bindings, *J. Chem. Inf. Model.*, 2021, **61**(8), 3891–3898, DOI: **10.1021/acs.jcim.1c00203**.

72 N. Eswar, B. Webb, M. A. Marti-Renom, M. S. Madhusudhan, D. Eramian, M. Y. Shen, U. Pieper and A. Sali, Comparative protein structure modeling using Modeller, *Curr. Protoc. Bioinf.*, 2006, DOI: **10.1002/0471250953.bi0506s15**.

73 **https://www.3ds.com/products-services/biovia/products/molecular-modeling-simulation/biovia-discovery-studio/visualization/**.

74 L. Ivanova, J. Tammiku-Taul, A. T. García-Sosa, Y. Sidorova, M. Saarma and M. Karelson, Molecular Dynamics Simulations of the Interactions between Glial Cell Line-Derived Neurotrophic Factor Family Receptor GFRα1 and Small-Molecule Ligands, *ACS Omega*, 2018, **3**(9), 11407–11414, DOI: **10.1021/acsomega.8b01524**.

75 P. Broto, G. Moreau and C. Vandycke, Molecular structures: perception, autocorrelation descriptor and sar studies. Autocorrelation descriptor, *Eur. J. Med. Chem.*, 1984, **19**, 66–70.

76 **https://www.epa.gov/sites/default/files/2015-05/documents/moleculardescriptorsguide-v102.pdf**.

77 O. Devinyak, D. Havrylyuk and L. Roman, 3D-MoRSE descriptors explained, *J. Mol. Graphics Modell.*, 2014, **54**, 194–203, DOI: **10.1016/j.jmgm.2014.10.006**.